A digital twin-based adaptive optimization approach applied to waste heat recovery in green steel production: Development and experimental investigation

Lukas Kasper [a],*, Paul Schwarzmayr [a], Felix Birkelbach [a], Florian Javernik [b], Michael Schwaiger [b], René Hofmann [a]

[a] *TU Wien, Institute of Energy Systems and Thermodynamics, Getreidemarkt 9/BA, 1060 Vienna, Austria*
[b] *voestalpine Stahl Donawitz GmbH, Kerpelystraße 199, 8700 Leoben, Austria*

ARTICLE INFO

ABSTRACT

Renewable-dominated power grids will require industry to run their processes in accordance with the availability of energy. At the same time, digitalization introduces new possibilities to leverage the untapped optimization potential to provide this flexibility. Mathematical optimization methods such as mixed-integer linear programming (MILP) are widely used to predict optimal operation plans for industrial systems. MILP models are difficult to adapt, but the viability of the predicted plans relies on accurate underlying models of the actual behavior. New automation paradigms, such as the digital twin (DT), can overcome these current drawbacks. In this work, we present the implementation and experimental evaluation of several micro-services on a standardized five-dimensional DT platform that automate MILP model adaption and operation optimization. These micro-services guarantee that, (1) deviations between the physical entity and its virtual entity models are detected, (2) the models are adapted accordingly, (3) subsequently linearized to suit the MILP approach and (4) used for live operational optimization. These novel services and DT workflows that orchestrate them were experimentally tested with a packed bed thermal energy storage (PBTES) test rig that acts as a physical entity. A waste heat recovery use case in steel production is used as the evaluation scenario. While the model error of a static simulation model would increase to 60% over 7 days of operation, the model error remains well below 25% as a result of successful model adaption. The prediction error of the optimization model remains in a typical magnitude of 10 to 20% during the evaluation period, despite the degradation of the PBTES power.

1. Introduction

1.1. Motivation

Heat generation in the industry sector accounts for roughly 20% of global anthropogenic CO_2 emissions [1]. This ratio increases to over 40% of total emissions [2] when also emissions related to the industry's electricity demand are allocated to it. Tremendous efforts are made to reduce these emissions and thus mitigate environmental impact. A major lever for this is reducing primary energy consumption through energy efficiency measures. Waste heat recovery, e.g., by using thermal energy storage (TES) for decoupling energy supply and demand, is considered a key aspect [3]. Yet, Martin & Chiu [4] found that the industry still restrains from TES application due to (1) economic feasibility, and (2) increased complexity to processes, hence increased

operational risk. Thus, optimal utilization of TES potential is required, and, therefore, modeling and optimization of energy systems is crucial. Accurate models are key to guarantee optimized operation. In industrial plants, highly individualized components are operated under harsh conditions, leading to changing properties and behavior. Therefore, the automated adaption of complex operational optimization models remains a challenging task.

1.2. Background

1.2.1. Operational optimization of energy systems

Optimal control of industrial energy system operation is typically realized via at least two automated control layers [5]. Basic process control, via, e.g., proportional–integral–derivative (PID) controllers, is

---

Nomenclature

Acronyms

BPMN	Business Process Model and Notation
DH	District heating
DT	Digital twin
EAF	Electric arc furnace
GDTA	Generic Digital Twin Architecture
IoT	Internet of Things
LD	Linz-Donawitz
MILP	Mixed-integer linear programming
MPC	Model predictive control
MQTT	Message Queuing Telemetry Transport
OBDA	Ontology-Based Data Access
OPC UA	Open Platform Communications Unified Architecture
PBTES	Packed bed thermal energy storage
PID	proportional–integral–derivative (controller)
PLC	Programmable Logic Controller
RSS	Ruths steam storage
SCADA	Supervisory control and data acquisition
SG	Steam generator
SH	Steam superheater
SOC	State of charge
SPARQL	SPARQL Protocol and RDF Query Language
SQL	Structured Query Language
TES	Thermal energy storage
TTT	Tap-to-tap (referring to EAF cycle)
UC	Unit commitment
VES	Virtual energy system

Indices

i	Index in sum
j	Time step with fixed electricity values
k	Index in sum
n	Number of time steps/ measurement values
t	Time step
u	Unit index
b	bottom
ch	Superscript - charging
crit	Superscript - critical value
dis	Superscript - discharging
el	Superscript - electric
fixed	Superscript - fixed value
gas	Superscript - gas burner
init	Initial value
lat	lateral
loss	Superscript - losses
max	Superscript - maximum value
min	Superscript - minimum value
out	Superscript - outgoing power
proc	Superscript - process demand
ramp	Superscript - ramping parameter

sat	Superscript - saturation
slack	Superscript - slack variable
t	top
turb	Superscript - steam turbine

Parameters and Variables

Δt	Time step size
$\dot{Q}$	Parameter - thermal power
$\dot{q}$	Continuous variable - thermal power
η^+	charging efficiency
η^-	discharging efficiency
γ^{TES}	Thermal loss factor of TES
λ_{pb}	effective thermal conductivity of packed bed
$\mathcal{J}$	Set of discrete time steps
$\mathcal{T}$	Set of discrete time steps
$\mathcal{U}$	Set of units in the UC problem
θ	Parameter array (optimization variables)
$\tilde{\theta}$	Optimized parameters
A^{slack}	slack parameter
C	Parameter - costs
e	Error term
h	Continuous variable - SOC auxiliary variable
J	Objective function
k	heat transfer coefficient
p	Continuous variable - electric power
S	Parameter - state of charge
s	Continuous variable - state of charge
T^{spread}	Temperature spread at the PBTES outlet
w	Weighting factor
x	Binary variable - on/off
z	Binary variable - TES state

Symbols

f	linear function

economically timed operation of energy supply, storage, and consumption for a prediction horizon of hours to months. The UC problem, originating in electric power system research [7], has also been widely applied to thermal processes [8], where it is also often referred to as energy management problem [9,10]. We refer to this higher level of economic process control as operational optimization. Even higher-level operational planning was proposed, considering production scheduling on larger time scales. For example, Gan et al. [11] presented a three-stage approach for economic operation of a steel plant, and Zhang & Grossman [12] reviewed options for enterprise-wide optimization for industrial demand side management. UC problems have also been applied considering the economic incentives of electricity markets at different timescales, see, e.g., Dowling et al. [13].

Various methods have been proposed to solve UC problems, such as, for example, heuristic priority listing, dynamic programming, Lagrangian relaxation, simulated annealing, fuzzy logic, artificial neural networks, genetic algorithms, and linear and mixed-integer linear programming (MILP) [5]. Moser et al. [9] state that modern energy management is most commonly based on MILP. A MILP problem is a mathematical optimization problem featuring a linear objective function and linear inequality constraints on the variables, which can be either continuous or integer-valued. The main benefit of MILP is the existence of powerful solvers, which can solve even large optimization problems in a reasonable time and are accessible from almost

applied for the low-level realization of system states and must account for fast dynamics and possible disturbances [6]. On a higher level, typically unit commitment (UC) problems are solved to decide on the

any programming language [9]. Furthermore, MILP avoids the risk of terminating at non-global minima, associated with non-linear optimization [14]. The problem of highly nonlinear dependencies has been partly solved by numerous piecewise linear approximations applicable to energy system components that have been proposed in recent years (see, e.g., [15–17]).

Despite the successful demonstration of MILP implementations for various applications, a major handicap is that the outcome of optimization heavily relies on the accuracy of the underlying models. Especially in energy systems, components are subjected to harsh environments leading to changing component behavior and often performance degradation. Examples include the aging or erosion of regenerative heaters in thermal power plants [18], fouling [19] and erosion of heat exchangers [20], degradation of electrode material [21], wear of rotating machinery [22], dust accumulation on photovoltaic modules [23], the load degradation of fuel cells [24,25], degradation of electric batteries [26], and, the degradation of storage material in latent [27] and sensible thermal energy storage [28].

Under these conditions, adaptive modeling and optimization provides huge benefits for energy system operation. Pattison et al. [29] presented a framework to identify low-order dynamic process models, later called "scale-bridging models", directly from historical process transition data. These models are used to connect the disparate time scales between the scheduling and control layers by mapping inputs (imposed by the scheduling layer) to the process outputs (dynamic response of selected process variables) [30]. This work was later extended by Kelley et al. [31] who presented a set of reformulation and linearization techniques to approximate the problem as MILP problem. Adaptive schemes have also been proposed in the control engineering community. Lu et al. [32] proposed a robust model predictive control (MPC) algorithm, incorporating online model adaptation. Adetola et al. [33] presented a closed-loop parameter estimation routine for MPC. However, in a review on industrial practices, Forbes et al. [34] examined a lack of implementation. They state that the concerns of industry have shifted away from pure MPC performance to how easily it can be installed, how intuitively operators can interact with it, and how long-term performance can be monitored and maintained with limited resources. This is where digital twin (DT) technology could be a practical enabler [35], since it promises a new level of automation and ease of implementation.

1.2.2. Digital twin technology in the energy sector

The DT concept has received increasing attention over the last few years [36]. While there exist many different definitions [37,38] and industrial application scenarios [39], one of the key pillars of DT technology is keeping digital representations of real-world plants in sync with their physical counterparts [40,41]. In contrast to a simple virtual representation (i.e., a model), a DT features automated bidirectional information and data exchange between the real and virtual systems [40].

These characteristics make a DT perfectly suited to meet the challenge of adaptive operation optimization of industrial energy systems introduced above. According to a recent review by Yu et al. [36], DT technology could fundamentally change the way industrial energy systems operate. The promise of DTs is to increase automation and deliver more intelligent and efficient operation. Compared to adaptive MPC algorithms and automated model identification approaches, briefly mentioned in the previous subsection, DT technology could be located at a higher level of automation. Encompassing advanced prediction, control and optimization techniques, the consistent application of DT frameworks should ensure ease of implementation, scalability, and interoperability of such methods in the form of services.

Yu et al. [36] concluded that adaptive DT technology for real-world behavior changes is still a critical future research direction. However, in a recent review on DT in the energy industry, Sleiti et al. [42] found that DT research related to the energy sector is still in its infancy

stage. Most crucially, the majority of proposed DT in the energy domain lack automated bidirectional connectivity between virtual and physical entity [36]. Therefore, real-world demonstration of "complete" DTs in the energy domain is pivotal, and implementation templates are necessary to foster implementation.

1.3. Scope of this work

Based on the state of the art, outlined above, the necessity for adaptive modeling methodologies is clear. These are especially valuable for the operational optimization of industrial energy systems due to the huge potential for reducing energy demand and CO_2 emissions. The state-of-the-art approach for such economic operation problems is MILP [9,43]. DT technology could greatly facilitate updating MILP models of physical components according to current behavior. A DT platform, however, needs to be equipped with appropriate functionality encapsulated in DT services. To the best of our knowledge, there is no literature available on the topic of achieving this automated adaptivity using a DT. Therefore, we continue our previous work on DT technology for industrial energy systems and determine which services are needed for fulfilling this application scenario and how they are composed. We further elaborate on the data transfer within the DT platform and the necessary workflow connectivity between the services. We present proof of the feasibility of the presented approach via experimental investigation on a PBTES test rig, emulating an industrial use case in steel production.

The novelty of this work can be summarized as follows: We

- present a DT-based approach to achieve adaptive TES modeling and MILP-based optimization,
- establish the set of DT services necessary to provide these automated adaptation capabilities,
- introduce a use case of TES integration in steel production that requires real-time adaptive optimization for energy-efficient operation, and,
- test and validate the developed approach in live operation on a packed bed TES test rig, emulating the use case.

1.4. Paper structure

After this introduction, this paper is organized as follows: Section 2 presents the industrial use case in steel production (Section 2.1), which provides means of evaluation of this work and briefly explains the DT platform (Section 2.2) that provides the foundation for this work. It furthermore introduces the TES test rig the DT is applied to (Section 2.3), and a state-of-the-art UC problem of the use case (Section 2.4), modeled via MILP. The novel DT-based methodology is presented in Section 3 and the experimental results of its application are given in Section 4. After this, Section 5 gives a brief conclusion of this work and an outlook on further research.

2. Material and methods

2.1. Industrial energy system use case

The considered use case in this paper is a steel production process and the subsequent off-gas heat recovery. The iron and steel industry accounts for approximately 8% of annual global anthropogenic CO_2 emissions [44]. These emissions must be reduced drastically to realize the current 1.5 °C goal defined in the Paris Agreement. That is, despite the International Energy Agency's predicted growing steel demand from around 1.9 billion tons in 2019 to over 2.5 billion tons in 2050 [45]. Therefore, breakthrough decarbonization technologies, such as electric arc furnaces (EAF) are essential [46]. However, still roughly a third of the total energy input is leaving the EAF via the sensible heat of the off-gas [47,48]. Therefore, there is immense potential for energy recovery [49]. Given the substantial costs associated with implementing
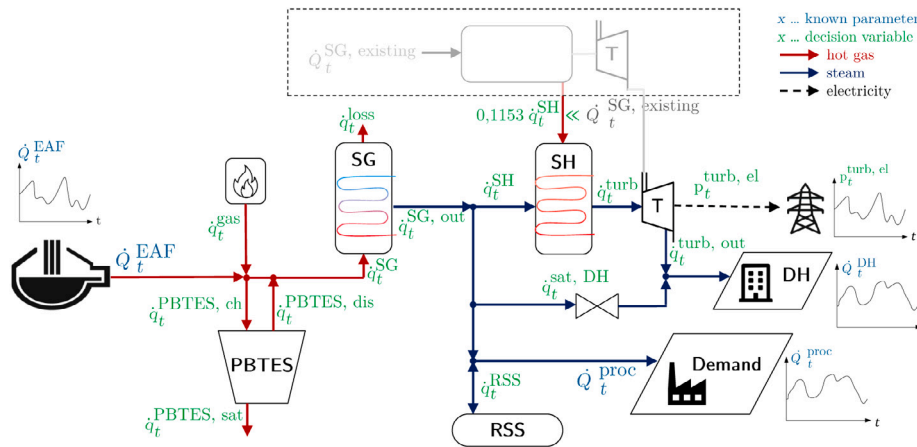
Fig. 1. Sketch of the industrial use case that is modeled as a virtual energy system in this work.

new low-emission strategies, a viable approach for operators of steel plants to significantly progress towards eco-friendly steel production is by installing heat recovery systems [48]. For an overview of waste heat recovery in the iron and steel industry, we refer to a recent analysis of Inayat [50].

The Austrian company *voestalpine Stahl Donawitz GmbH* recently announced the construction approval of a new EAF at their site in Leoben, Austria, as part of their "greentec steel" transformation path [51].

The company's goal is a reduction of 30% of the current CO_2 emissions from 2027 onward, and CO_2-neutral steel production by 2050. The first transformation step sees one of the two current steel routes, with a blast furnace and an LD converter each, replaced by an EAF. In this paper, we therefore consider the heat recovery process of the EAF route individually, albeit it will be connected to the existing industrial energy system at the site. This corresponds to the current medium-term adaption plans.

In the considered energy system use case, illustrated in Fig. 1, the thermal energy of the hot off-gas of the EAF is recovered in a waste heat boiler. A similar system, specifically designed for steam generation of EAF off-gas, was designed by Steinparzer et al. [52] as a five-pass system including radiation passes, evaporation panels, evaporation bundles, and an economizer for preheating feed-water. We will reduce this system to its basic purpose from here on and simply call it steam generator (SG). The generated steam is valuable for multiple purposes. Firstly, a large amount of saturated steam is needed for further metal processing at the site. Secondly, lower-temperature heat can be decoupled from the steam system to provide facility heating on-site and district heating for the adjoining city. Thirdly, saturated steam can be superheated in the existing SG and fed into a turbine to produce electricity. Since the EAF operates as a batch process, its hot off-gas flow features not only high volatility but also periods of disruption [52,53]. The SG, on the other hand, must adhere to power ramping constraints and should ideally never be shut down completely. Subjecting a SG to overly fluctuating input power can lead to excessive material stresses due to pressure and temperature gradients, and a wide range of other potentially life-limiting factors within the system [54]. Steinparzer et al. [52] and Keplinger et al. [48] argue that this challenge should be solved by integrating a TES between the EAF and the SG. During off-gas peaks, the TES can be charged, and during EAF downtimes or periods of lower heat flow occur, e.g., during initial raw material heating, the TES can be discharged to provide steady input power to the SG. Manente et al. [55] recently presented a procedure to identify the best TES option for the heat recovery of discontinuous flue gas in steel production for steam generation. They found that a packed bed thermal energy storage (PBTES) using rocks as a storage medium is the optimal choice from a techno-economic perspective.

Thus, in our use case a PBTES is considered to smoothen the volatile EAF off-gas flow, hence accommodating the load requirements of the SG. Comprehensive reviews on this type of TES technology can be found in the work of Gautam et al. [56,57] and Xie et al. [58].

Another major challenge for EAF heat recovery systems are the high gas velocities in the inlet duct and the high dust load of the EAF exhaust gases [52]. While high gas velocities lead to increased surface erosion [20], they can also be leveraged to achieve higher heat transfer. The problem can be modulated with the design (e.g., cross sections) of pipes and heat exchangers. For example, Marti et al. [59] conducted a PBTES design optimization considering different velocities and the induced pressure drop at different cross-sections. Bause et al. [60] states a typical iron oxide dust concentration in EAF off-gas of $20\,g/Nm^3$. Put another way, about 15 to 25 kg of dust per ton of produced steel accumulates [61]. Typically, this is why a drop-out box is arranged after the inlet duct of the hot gas line, which separates the coarse dust particles by gravitation [49,62]. However, the majority of the EAF dust consists of particles below a size of $20\,\mu m$ [61]. This raises the question of how the dust-laden exhaust gas used as heat transfer fluid (HTF) will affect the PBTES performance. Investigations are currently underway to quantify this behavior [63], but it can be expected that the small particles accumulate in the packed bed of the PBTES [64]. It is well known that dust deposits increase the air pressure drop across a packed bed [65,66]. Thus, we deduce that the available PBTES charging/discharging power rates will gradually decrease based on the dust-induced pressure drop and a maximum air fan power at the end of the hot gas duct. This is a major effect besides, e.g., the degrading heat capacity of PBTES storage media [28]. These degradation effects not only lead to design challenges for the heat recovery system but also call for intelligent operation approaches that consider the reduced PBTES power.

2.2. Digital twin platform

The foundation of our DT approach is the DT platform developed in previous work, building on the Generic Digital Twin Architecture (GDTA) [67]. The DT platform was introduced by Kasper et al. [68]. Furthermore, Schwarzmayr et al. [69] presented the instantiation of the DT platform on the PBTES test rig, introduced in Section 2.3.

The instantiated DT platform is illustrated in Fig. 2. It follows the basic five-dimensional DT concept introduced by Tao et al. [70]. Accordingly, it consists of (1) the physical entity, (2) the virtual entity, (3) the connection dimension, (4) the data dimension, and (5) the service dimension. The physical entity is connected to the virtual space via programmable logic controllers (PLC)s and the supervisory control and data acquisition (SCADA) system. New data points are sent to the message broker (connection dimension) and control signals are
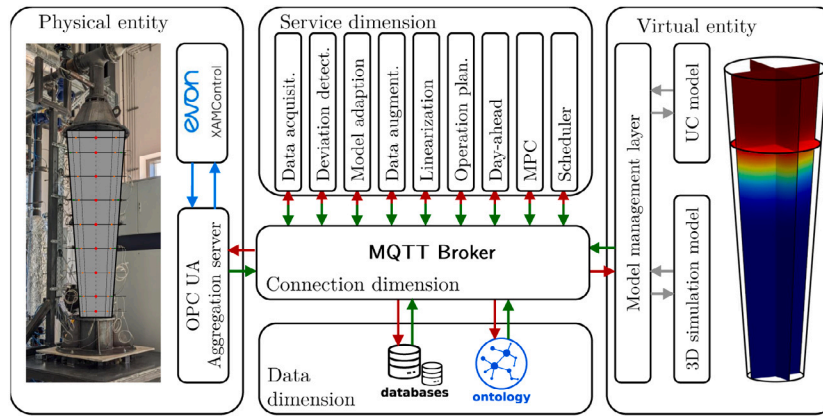
Fig. 2. Five-dimensional DT platform implemented for the PBTES test rig.
Source: Adapted from the author's previous publication [69].

received. The virtual entity should be able to accurately represent the behavior and properties of the physical entity. This can be fulfilled by various types of virtual models. The data dimension provides semantic structuring of all data in the DT platform and a central access point for decentralized data storage. At the core of it is a knowledge graph (see, e.g., [71]), consisting of several ontologies and a built-in reasoner. We applied the Ontop framework [72] for this. With our implementation of the data dimension, it is possible to query and receive any information within the scope of the DT from a single endpoint using SPARQL Protocol and RDF Query Language (SPARQL). The aim of the service dimension is to encapsulate various functionalities of the DT into micro-services that provide user-friendly interfaces and allow easy on-demand use and adaption. The timely and sequential coordination of various service instances is realized with a service orchestrator. We use a workflow engine, based on Business Process Model and Notation (BPMN) workflows for this.

For more details on the DT platform, we must refer to our previous publications [68,69].

2.3. Packed bed thermal energy storage test rig

A lab-scale test rig of a PBTES is used for experimental evaluations in this work. The test rig, situated at the laboratory of TU Wien, consists of a vertically standing steel vessel that is filled with slag as storage material. The slag, a by-product from the iron and steel industry, is chosen as storage material because of its thermo-physical properties and low costs. It consists of irregularly shaped porous rocks which leads to an enhanced heat transfer between storage material and HTF and results in an even and homogeneous perfusion of the packed bed. To minimize heat losses to the surrounding the storage vessel and all piping is insulated with multiple layers of ceramic wool, rock wool, and aluminum sheeting. For charging and discharging, the test rig can be supplied with air from an air supply unit (ASU). Air temperatures from $20\,°C$ to $400\,°C$ and a mass flow of $100\,\mathrm{kg\,h^{-1}}$ to $400\,\mathrm{kg\,h^{-1}}$ are available. To measure the current state of the storage, the test rig is equipped with multiple temperature and differential pressure sensors. Detailed descriptions of the test rig, its instrumentation, and the properties of the used materials can be found in the studies of Schwarzmayr et al. [69,73]. Fig. 3 shows the PBTES test rig with and without insulation as well as a photograph of the storage material.

To charge the test rig, the ASU provides hot air that enters the storage from the top, passes through the packed bed, thereby delivering heat to the storage material, and exits the storage at the bottom. To recover the heat stored in the TES, the ASU provides cold air that passes through the packed bed in the opposite direction and is thereby heated. Due to physical restrictions of the ASU, a 15 minute downtime between charging and discharging periods has to be maintained.
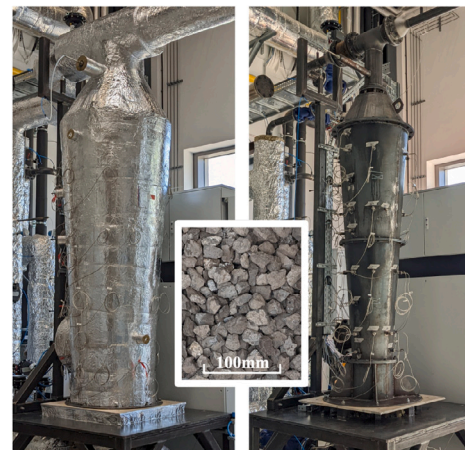

Fig. 3. Test rig of a PBTES at the laboratory of TU Wien: with thermal insulation (left), storage material (center), without thermal insulation (right).
Source: Reprinted from [73] with permission from Elsevier.

These downtimes are necessary to preheat/precool the ASU so that it can deliver the HTF temperatures that are required for charging and discharging the storage. In reality, the HTF used to charge the TES will be accompanied by a significant amount of metal-oxide dust. As explained in Section 2.1, this will lead to a gradual degradation of the thermal performance of the PBTES. To simulate this effect of gradual degradation of the thermal performance in the laboratory setup, the HTF mass flow that is requested from the ASU is scaled with a factor that is smaller than one and gradually decreases over time.

2.3.1. Packed bed thermal energy storage operating behavior

The PBTES' charging and discharging power depend on the temperature spread of the in- and out-flowing HTF. This temperature spread decreases towards the end of a cycle, hence thermal power is decreasing. During charging, we speak of saturation of the out-flowing HTF, and these saturation losses must be taken into account in operation in addition to the decreasing charging power. Furthermore, Koller et al. [17] showed that under dynamic operation, the PBTES power is not only dependent on the current SOC but also on the SOC at the end of the previous charging or discharging phase. To model partial cycle operation, also the initial SOC at the end of the previous charging or discharging phase must be taken into account. This behavior is illustrated in Fig. 4.
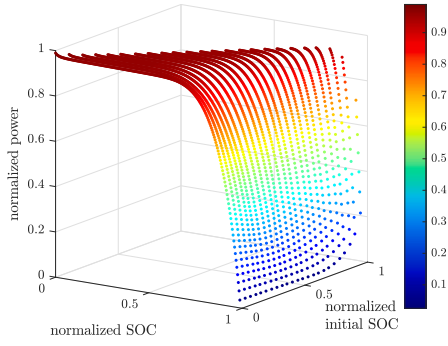
Fig. 4. Dependency of the maximum charging power of a PBTES on the current SOC and the initial SOC at the last operation switch. The maximum discharging power features an equivalent but inverse dependency on the SOC.

2.4. Unit commitment model for the virtual energy system

The waste heat recovery use case, introduced in Section 2.1, is modeled via MILP. The UC model is illustrated in Fig. 1 together with relevant power variables. Here, the basic assumptions and fundamental modeling approaches are presented. In the remainder of this paper, we refer to this virtually modeled industrial use case as the virtual energy system (VES). In this paper, we consider the design of the VES as fixed. The design is not optimized but reasonable parameters were chosen, which are given in Appendix B. The evaluation input data is given in Appendix A.

The VES is modeled in a unit commitment (UC) formulation within a finite number n of discrete time steps $t \in \mathcal{T} = \{t_1, \ldots, t_n\}$ at an equidistant time step width Δt. Energy flows in the VES are reduced to heat flows, i.e., neglecting temperature levels. This is a common approach in UC problems of industrial energy systems (see, e.g., [74,75]), where temperature levels are considered at lower hierarchy control layers. Therefore, each unit $u \in \mathcal{U}$ is modeled via its thermal power $\dot{q}_t^u \in \mathbb{R}$ as decision variable in each time step. In this paper, decision variables are distinguished by lowercase writing and parameters are written in uppercase.

2.4.1. Basic unit power constraints

Some units are modeled with maximum ramping rates, hence their power is constrained between their minimum and maximum power $(\dot{Q}_{\min}^u, \dot{Q}_{\max}^u)$ by

$$x_t^u \dot{Q}_{\min}^u \leq \dot{q}_t^u \leq x_t^u \dot{Q}_{\max}^u \quad \forall t \in \mathcal{T} \ , \tag{1}$$

with the binary decision variable $x_t^u \in \{0, 1\}$ denoting the on/off state of the unit u at a timestep t. The ramping constraints are then given as

$$
\begin{aligned}
&- \Delta \dot{Q}_{\text{ramp}}^u + \left(x_t^u - x_{t-1}^u\right) \left(\frac{\dot{Q}_{\min}^u}{\Delta t} - \Delta \dot{Q}_{\text{ramp}}^u\right) \\
&\leq \frac{\dot{q}_t^u - \dot{q}_{t-1}^u}{\Delta t} \leq \\
&- \Delta \dot{Q}_{\text{ramp}}^u + \left(x_t^u - x_{t-1}^u\right) \left(\frac{\dot{Q}_{\max}^u}{\Delta t} - \Delta \dot{Q}_{\text{ramp}}^u\right) \\
&\forall t \in \mathcal{T} \ ,
\end{aligned}
\tag{2}
$$

with, in this case, direction-independent maximum ramping rates $\Delta \dot{Q}_{\text{ramp}}^u$. Note, that the initial states $x_{t=0}^u$ and $\dot{q}_{t=0}^u$ must be provided.

For units featuring no ramping constraints and no minimal partial load (i.e. $\dot{Q}_{\min}^u = 0$), Eqs. (1)–(2) can be reduced to

$$\dot{Q}_{\min}^u \leq \dot{q}_t^u \leq \dot{Q}_{\max}^u \quad \forall t \in \mathcal{T} \ . \tag{3}$$

2.4.2. Storage formulation

The two TES units in this use case are modeled via a basic storage formulation, constraining the charging/discharging power rate $\dot{q}_t^{\text{TES}}$ via

$$-\dot{Q}_{\max}^{\text{TES}} \leq \dot{q}_t^{\text{TES}} \leq \dot{Q}_{\max}^{\text{TES}} \quad \forall t \in \mathcal{T} \tag{4}$$

to a maximum available charging/discharging power rate $\dot{Q}_{\max}^{\text{TES}}$. Their state of charge (SOC) s_t^{TES} is constrained via

$$0 \leq s_t^{\text{TES}} \leq S_{\max}^{\text{TES}} \quad \forall t \in \mathcal{T} \tag{5}$$

to the TES unit's capacity $S_{\max}^{\text{TES}}$. The SOC changes are modeled neglecting conversion efficiencies which are assumed near one, but considering a thermal loss factor γ^{TES}. The factor expresses the ratio of the current SOC that dissipates through thermal losses during the time Δt. This results in the following set of equations:

$$s_{t+1}^{\text{TES}} = s_t^{\text{TES}} \left(1 - \gamma^{\text{TES}} \Delta t\right) - \dot{q}_t^{\text{TES}} \Delta t \quad \forall t \in \mathcal{T} \tag{6}$$

Note that the TES power rate is defined as negative when the storage is charged and that the final SOC $s_{t_{n+1}}^{\text{TES}}$ must be defined appropriately, so as not to discharge the storage completely at the end of the prediction horizon. The initial SOC value $s_{t_1}^{\text{TES}}$ is always set to the current SOC of the TES.

2.4.3. Packed bed thermal energy storage modeling

For the PBTES test rig, the basic storage constraints are extended with a formulation developed by Koller et al. [17] to account for the nonlinear charging/discharging power rate dependency on the SOC, and for saturation losses during the charging process.

The charging/discharging power rate $\dot{q}_t^{\text{TES}}$ of the PBTES, constrained by the basic formulation (see Section 2.4.2), is split into charging power $\dot{q}_t^{\text{PBTES, ch}}$ and discharging power $\dot{q}_t^{\text{PBTES, dis}}$, i.e.,

$$\dot{q}_t^{\text{TES}} = \dot{q}_t^{\text{PBTES, dis}} - \dot{q}_t^{\text{PBTES, ch}} \quad \forall t \in \mathcal{T} \ . \tag{7}$$

The binary variables $z_t^{\text{PBTES, ch}}$, $z_t^{\text{PBTES, dis}} \in \{0, 1\}$ are defined to take the value 1, if the PBTES is in charging or discharging state, respectively. Since our PBTES test rig features a minimum charging/discharging power $\dot{Q}_{\min}^{\text{PBTES}}$ due to limitations of the air supply unit, we introduced the minimum partial load constraints

$$
\begin{aligned}
z_t^{\text{PBTES, ch}} \dot{Q}_{\min}^{\text{PBTES}} &\leq \dot{q}_t^{\text{PBTES, ch}} \\
&\leq z_t^{\text{PBTES, ch}} \dot{Q}_{\max}^{\text{PBTES}} \quad \forall t \in \mathcal{T} \ ,
\end{aligned}
\tag{8}
$$

$$
\begin{aligned}
z_t^{\text{PBTES, dis}} \dot{Q}_{\min}^{\text{PBTES}} &\leq \dot{q}_t^{\text{PBTES, dis}} \\
&\leq z_t^{\text{PBTES, dis}} \dot{Q}_{\max}^{\text{PBTES}} \quad \forall t \in \mathcal{T} \ .
\end{aligned}
\tag{9}
$$

In case the TES unit features a continuous power range, the left-hand side inequalities in Eqs. (8) and (9) can be skipped.

The charging power is then constrained by

$$
\begin{aligned}
\dot{q}_t^{\text{PBTES, ch}} &\leq f^{\text{ch}} \left(\frac{s_t^{\text{TES}} + s_k^{\text{TES}}}{2}, h_t^{\text{ch}}, z_t^{\text{PBTES, ch}}\right) \\
&\quad \forall t \in \mathcal{T}, \ k = \min\{t+1, t_n\} \ ,
\end{aligned}
\tag{10}
$$

and the discharging power is constrained analogously with f^{dis}. Here, f^{ch} and f^{dis} are linear functions of the stated decision variables. The auxiliary variables h_t^{ch} and h_t^{dis} represent the SOC at the end of the previous charging/discharging switch. For details on this formulation, which we consider too comprehensive to recapitulate, as well as for the constraints on the auxiliary variables h_t^{ch}, h_t^{dis}, we refer to Koller et al. [17].

The UC problem is further extended by the saturation losses $\dot{q}_t^{\text{PBTES, sat}}$, which are constrained by

$$
\begin{aligned}
\dot{q}_t^{\text{PBTES, sat}} &\geq f^{sat} \left(\dot{q}_t^{\text{PBTES, ch}}, z_t^{\text{PBTES, ch}}, T_t^{\text{spread}}\right) \\
&\quad \forall t \in \mathcal{T} \ ,
\end{aligned}
\tag{11}
$$

with the linear function f^{sat} of the given decision variables. Here, T_t^{spread} denotes the temperature spread at the PBTES outlet that can be constrained with the same linearized formulation as given in f^{ch}, albeit weighted to the maximum temperature spread instead of the maximum charging power. For details, we again refer to the original publication: [17]. To account for the limit in the total heat flow introduced to the PBTES during charging, we constrain $\dot{q}_t^{\text{PBTES, ch}}$ and $\dot{q}_t^{\text{PBTES, sat}}$ to the maximum available charging power of the PBTES:

$$0 \leq \dot{q}_t^{\text{PBTES, ch}} + \dot{q}_t^{\text{PBTES, sat}}$$
$$\leq z_t^{\text{PBTES, ch}} \dot{Q}_{\max}^{\text{PBTES}} \quad \forall t \in \mathcal{T} . \tag{12}$$

In contrast to Koller et al. [17], we do not implement the formulation for a minimum temperature requirement of gas stream mixing after the PBTES for the sake of simplicity of the UC model. However, this implementation would be straightforward. This simplification does not affect the evaluation in this Paper but should be considered for applications that are sensitive to temperature levels.

2.4.4. Minimum downtime

The operation of our PBTES test rig must abide by a minimal downtime of 15 minutes between switches from charging to discharging and vice versa. This is due to limitations in the air supply unit, as presented in Section 2.3. Whenever the PBTES switches to idle mode, a bypass mode is activated to pre-heat or cool the air supply unit. To account for the downtime requirement in the operation schedule, a standard minimal downtime formulation is added to the UC problem, see, e.g., [76].

2.4.5. Energy balances

On the hot gas side, illustrated on the left side of Fig. 1, the energy balance constraint

$$\dot{Q}_t^{\text{EAF}} + \dot{q}_t^{\text{gas}} = \dot{q}_t^{\text{PBTES, ch}} + \dot{q}_t^{\text{PBTES, sat}}$$
$$- \dot{q}_t^{\text{PBTES, dis}} + \dot{q}_t^{\text{SG}} + \dot{q}_t^{\text{loss}} \quad \forall t \in \mathcal{T} , \tag{13}$$

with $\dot{q}_t^{\text{loss}} \geq 0$ links the supply units with the PBTES and the SG. While the EAF waste heat flow $\dot{Q}_t^{\text{EAF}}$ is fixed, a conventional gas burner with thermal power $\dot{q}_t^{\text{gas}}$ provides flexibility on the hot gas side.

The SG is modeled to produce saturated steam $\dot{q}_t^{\text{SG, out}}$ with a constant efficiency η_{SG}, i.e.,

$$\dot{q}_t^{\text{SG}} = \frac{\dot{q}_t^{\text{SG, out}}}{\eta_{\text{SG}}} \quad \forall t \in \mathcal{T} . \tag{14}$$

A part of the saturated steam $\dot{q}_t^{\text{SH}}$ can be further superheated in an existing waste heat boiler on-site to provide superheated steam at $25\,\text{bar}_a$. For this, the energy balance

$$\dot{q}_t^{\text{turb}} = \dot{q}_t^{\text{SH}} \cdot 1.1153 \quad \forall t \in \mathcal{T} \tag{15}$$

holds.[1]

The turbine considered in our use case is an existing extraction condensation steam turbine. A part of the steam supplied to the turbine can be extracted at low pressure to satisfy heat demands, while the rest can be used for electricity generation through steam expansion. The extraction ratio can be varied, therefore the heat and electricity generation is decoupled [77]. Thus, the energy balance between the turbine input thermal power $\dot{q}_t^{\text{turb}}$ and the extracted heat $\dot{q}_t^{\text{turb, out}}$ and produced electricity $p_t^{\text{turb, el}}$ is modeled via the typical formulation [78]

$$\dot{q}_t^{\text{turb}} = \frac{\dot{q}_t^{\text{turb, out}}}{\eta_{\text{turb, out}}} + \frac{p_t^{\text{turb, el}}}{\eta_{\text{turb, el}}} \quad \forall t \in \mathcal{T} , \tag{16}$$

with the constant efficiencies for thermal power extraction $\eta_{\text{turb, out}}$ and electric generation $\eta_{\text{turb, el}}$. In case the electric turbine power was already committed on the market, it is fixed via

$$p_t^{\text{turb, el}} = P_t^{\text{el, fixed}} \quad \forall \{t \mid t \in T, j \in \mathcal{J} : t = j\} , \tag{17}$$

where $\mathcal{J}$ is the set of time steps for which a fixed electric power $P_j^{\text{el, fixed}}$ is given.

Within the saturated steam system, the energy balance constraint

$$\dot{q}_t^{\text{SG, out}} - \dot{q}_t^{\text{SH}} + \dot{q}_t^{\text{RSS}} =$$
$$\dot{Q}_t^{\text{proc}} + \dot{q}_t^{\text{sat, DH}} \quad \forall t \in \mathcal{T} \tag{18}$$

holds, with the RSS storage power $\dot{q}_t^{\text{RSS}}$, the fixed saturated steam demand for further production $\dot{Q}_t^{\text{proc}}$, and a proportion $\dot{q}_t^{\text{sat, DH}}$ (≥ 0) that can be used for additional district heating. Here, the district heating demand $\dot{Q}_t^{\text{DH}}$ is considered as a limit rather than a hard constraint, hence:

$$\dot{q}_t^{\text{sat, DH}} - \dot{q}_t^{\text{turb, out}} \leq \dot{Q}_t^{\text{DH}} \quad \forall t \in \mathcal{T} \tag{19}$$

Furthermore,

$$\dot{q}_t^{\text{SG, out}} - \dot{q}_t^{\text{SH}} \geq 0 \quad \forall t \in \mathcal{T} \tag{20}$$

ensures that no lower-pressure steam discharged from the RSS is considered to be fed back to the high-pressure system.

2.4.6. Objective function

The goal of the MILP UC problem of this use case is the maximization of the objective function

$$J_{\text{UC}} = \sum_{t \in \mathcal{T}} \left(C_t^{\text{el}} \cdot p_t^{\text{turb}} + C^{\text{DH}} \cdot \left(\dot{q}_t^{\text{sat, DH}} + \dot{q}_t^{\text{turb, out}} \right) \right.$$
$$\left. - C^{\text{gas}} \cdot \frac{\dot{q}_t^{\text{gas}}}{\eta_{gas}} - c_t^{\text{slack}} \right) , \tag{21}$$

which consists of the reward from electricity and district heating sales less the costs for the auxiliary gas burner, considering the price parameters C_t^{el}, C^{DH}, and C^{gas}. Additionally, a slack variable c_t^{slack} is added for the implementation of additional operational penalties. In this use case, the soft constraints

$$c_t^{\text{slack}} \geq A^{\text{slack}} \left(S_{\text{crit}}^{\text{TES}} - s_t^{\text{TES}} \right) \tag{22}$$

$$0 \leq c_t^{\text{slack}} \tag{23}$$

are added to penalize the violation of a critical RSS storage level $S_{\text{crit}}^{\text{TES}}$ with a slack parameter A^{slack}.

2.5. Simulation of the virtual energy system

In our experimental operation, only the PBTES is physically operated, while the rest of the VES needs to be simulated. The PBTES power values during real operation can never exactly match the operation plan resulting from the MILP UC problem. Combining the actual PBTES power values with the VES operation plan of the remaining (virtual) components during the same time period would conflict with the energy balances given in Section 2.4.5. Thus, we emulate a low-level control procedure, to comply with the energy balances in the resulting simulated VES operation.

This low-level control procedure is based on the same MILP constraints as the UC problem given in Section 2.4 with the PBTES power values fixed to those that were experimentally realized. However, the objective (see, Eq. (21)) is in this case not cost-efficient operation, but compliance with the previously predicted economic operation plan. Thus, the objective function consists of deviation terms of the planned power of VES units (gas burner, SG, RSS, and turbine) in the form of fixed parameters and the to-be-determined power of these units as variables. The individual deviation terms are weighted appropriately.

---

[1] A ratio of 0.1153 of the saturated steam enthalpy is additionally supplied by the existing waste heat boiler superheater. This is considered small. The ratio is given by the enthalpy difference between saturated steam at $25\,\text{bar}_a$ and superheated steam at $25\,\text{bar}_a$ at $100\,\text{K}$ above the saturation point.

The minimization of this objective returns a "simulated" VES schedule that complies with the energy balances while maintaining cost-efficient trajectories.

This "simulation" procedure of the VES replicates the low-level control of units according to the operation schedule in a real energy system. The procedure was included as a preliminary step linked to and executed before the model predictive control (MPC) service is called. This service will be introduced in Section 3.1.7. When called, the described MILP UC problem is solved only for the current historic time period, which was not fixed via simulation yet.

The realized power values as well as the storage capacity of the PBTES test rig are scaled up in the VES by a constant factor. Equally, the results of the VES MILP UC problem are scaled down before scheduling power values on the test rig. This factor is 3 000 and resulted from the test rig's physical and operational constraints and a rough PBTES scaling in the use case.

3. Implementation

The five-dimensional DT platform first presented in [68] and briefly introduced in this paper in Section 2.2, was equipped with additional functionality in the form of micro-services and workflows to solve the problem statement given in Section 1.3.

All services were implemented in MATLAB® R2023b and/or Python 3.10 language and virtualized in encapsulated containers via Docker [79], using Docker Engine 20. For the services solving the MILP UC problem, the parser YALMIP [80] R20210331 was used and GUROBI® 10.0.0 was used as a solver. The physical machine that hosted all services is a 64-core Linux system (AMD EPYC 7702P) with 256 GB of RAM. For implementation details on the fundamental DT platform, we refer to our previous publications [68,69].

3.1. Digital twin micro-services

Services contain the main functionality within the DT platform, tailored to use-case-related objectives. Building on previous work, we developed additional micro-services. Seven services are fully functional while two services are currently only implemented as a mock-up. In the following section, the function of each service and the methods implemented therein are briefly explained.

3.1.1. Data acquisition service

While the SCADA system, considered as part of the physical entity [68], acts as the primary layer of data collection, the data acquisition service fulfills the purpose of data correction, enrichment, and storage.

In our implementation, this service calculates power rates of the charged and discharged HTF of the test rig and estimates the SOC of the PBTES as

$$SOC_i = \frac{\sum_{k=1}^{9} E_{i,k} - E_{SOC=0}}{E_{SOC=1} - E_{SOC=0}} \,, \tag{24}$$

where $E_{SOC=1}$ is the energy stored in a fully charged storage (constant charging temperature), $E_{SOC=0}$ is the energy of a fully discharged storage (constant discharging temperature) and $\sum_{k=1}^{9} E_{i,k}$ is the currently stored energy which is calculated as

$$E_{i,k} = m_k \, c \, T_{i,k} \,. \tag{25}$$

The index k in Eqs. (24) and (25) represents the nine vertical volume sections in which the storage volume is discretized according to temperature sensor positions. The energy $E_{i,k}$ of the volume section k is calculated as the product of the mass of storage material m_k, the specific heat capacity of the storage material c and the measured value of the temperature sensor $T_{i,k}$ located in this section.

Furthermore, the data acquisition service processes the operating states of the air supply unit and stores this information in an SQL database. Thus, services such as MPC and operation planning service can fetch initial states as well as information on remaining downtime or last switches (important for initializing the auxiliary variables of the SOC, h_t^{ch} and h_t^{dis}, see Section 2.4.3).

3.1.2. Deviation detection service

The deviation detection service is currently implemented as a mock-up on our DT platform. Methods for robust detection of deviations are in the development phase (see, [69]). The service's purpose is to detect any deviations between the observed behavior of the physical component and the models of its virtual entity. It has to detect deviations and, if they are considered significant, assess whether the cause is physical entity faults or virtual model drifts. Of course, also the classification of physical faults should be considered. For more complex procedures, a more separated functionality encapsulation could be helpful.

3.1.3. Model adaption service

The model adaption service is mainly based on experimental live data and a finite volume simulation model of the PBTES test rig. The finite volume simulation model was developed and validated by Schwarzmayr et al. [81] to be used as the virtual entity in a DT framework. The model adaption service takes temperature measurements from the PBTES test rig as initial values and a set of parameters

$$\theta = \{k_b, k_t, k_{lat}, \lambda_{pb}, k_{pb}, \eta^+, \eta^-\} \tag{26}$$

to predict/reconstruct the thermal behavior of the test rig for a given schedule. The set of parameters θ includes several heat transfer coefficients that describe the heat losses to the surrounding (k_b, k_t, k_{lat}), the effective thermal conductivity of the packed bed λ_{pb}, the heat transfer coefficient between HTF and storage material k_{pb} as well as thermal efficiencies η^+ and η^- for the charging and discharging process which are the most important for the evaluations in this study. These two efficiencies are defined as

$$\eta = \frac{\dot{Q}_{htf}}{\dot{Q}_{pb}} \tag{27}$$

where $\dot{Q}_{htf}$ is the thermal power rate that is expected to be delivered by the ASU and $\dot{Q}_{pb}$ is the actual power rate provided by the ASU. For a PBTES with a clean packed bed and no gradual degradation of the thermal performance, these two power rates are the same (neglecting heat losses) and the efficiency η is at a constant value of 1 for both charging and discharging. As the behavior of the physical entity does not change over time, this finite volume model with a static set of parameters will be able to predict the behavior of the physical entity with high accuracy.

However, in case the thermal behavior of the physical entity gradually degrades over time (as is the case in this study) the set of parameters θ needs to be constantly updated in order to fit the behavior of the finite volume model to the behavior of the physical entity. To do so, the model adaption service takes experimental data from the test rig for the last 12 h of operation and uses the finite volume model to reconstruct the experimentally measured behavior of the physical entity. To find the optimal set of parameters $\tilde{\theta}$ we solve the nonlinear optimization problem

$$\tilde{\theta} := \arg\left(\min_{\theta} J(\theta)\right) \tag{28}$$

with the objective function

$$J(\theta) = \sqrt{\frac{1}{n} \sum_{i=1}^{n} \left(w_T \, e_{T,i}^2 + w_{SOC} \, e_{SOC,i}^2\right)} \tag{29}$$

where $e_{T,i}$ is the error between measured and reconstructed temperatures in the packed bed and $e_{SOC,i}$ is the error between the measured and the reconstructed state of charge (SOC) of the TES. w_T and w_{SOC} are empirically determined weights that adjust the order of magnitudes of e_T and e_{SOC}. The optimization problem defined in Eq. (28) is solved

with MATLAB®'s nonlinear solver *fmincon* which is initialized with the set of parameters that was the result of the last optimization run. This guarantees fast and reliable convergence. The new optimal set of parameters $\tilde{\theta}$ found by the solver together with its time range of validity is stored in the DT's data dimension where it can be accessed by every service of the DT.

3.1.4. Data augmentation service

The data augmentation service is triggered whenever a virtual entity model was adapted by the model adaption service and acts as a preliminary step before the linearization service (see, Section 3.1.5). Since it would be unreliable to fit a piecewise-linearized model based on a small amount of historic data, we chose the approach to simulate the whole SOC operating range with the maximum mass flow of the PBTES with the current accurate finite volume model fetched from the virtual entity.

The service first simulates a complete cycle of the PBTES, i.e., charging from SOC = 0 until SOC = 1 is reached with the maximum available power, and equally for discharging. It then loops through an equally grided time array of the initial cycle, simulating charging/discharging starting at different SOC levels until the final SOC is reached. This approach provides a high-resolution data set of the PBTES behavior for subsequent linearization.

3.1.5. Linearization service

This service automates the fitting of MILP-suitable piecewise-linear models of nonlinear operational behavior of system components. The service is triggered when new data from the data augmentation service (see, Section 3.1.4) is available and provides a current accurate model for the operation planning service and MPC service. In our implementation, the nonlinear dependency of the maximum PBTES charging/discharging power (see Eq. (10)), as well as the dependency of the saturation losses on the state of charge (see Eq. (11)), is linearized. The approach is based on the model formulation presented by Koller et al. [17]. We implemented a novel algorithm developed by Birkelbach et al. [82] and published on GitLab [83] that provides robust fitting with hyperplanes in one or two convex regions. While Koller et al. manually fitted the linearization on the dataset, our linearization service can automatically choose the separation of the two convex regions and approximate them with hyperplanes. The hyperplane parameters are then converted to MILP constraints at the cost of additional binary variables and Big-M constraints. For details, we refer to Birkelbach et al. [82]. Furthermore, the service performs a basic feasibility check of the approximation in the operating region to guarantee that no infeasibility issues in the subsequent application of the models arise. Fig. 5 illustrates an exemplary linearization run of this service for the maximum PBTES charging power. We used a fixed number of ten hyperplanes for the approximation in the evaluation of this work.

3.1.6. Operation planning service

The operational optimization of the physical system is split into two parts: A higher-hierarchy operation planning service that provides an optimal operation plan on a multi-day time horizon, and a lower-hierarchy MPC service that provides fast optimal control of the VES. Both services build on the same MILP model formulation given in Section 2.4, but differ in the length of the forecast horizon and additional boundary conditions. Such hierarchical energy management or also multi-layer optimization was proposed by multiple authors in recent years (see, for example, Dias et al. [84], Fuhrmann et al. [85], Valibeygi et al. [86] or Polimeni et al. [87]). For demonstration purposes, we implemented a very basic hierarchical control strategy. For details on the current state of the art, we refer to the specialized literature given above.

In our implementation, the operation planning service is triggered every 6 h and optimizes the operational schedule for the next 48 h. The
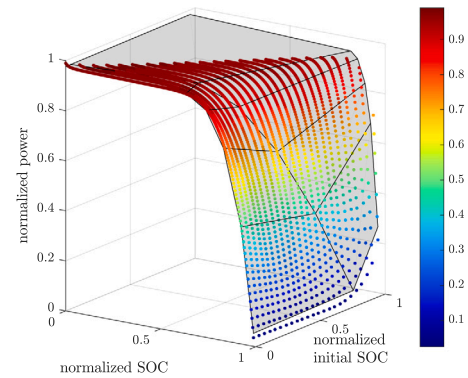

Fig. 5. Typical approximation of the nonlinear dependency of the maximum charging power of the PBTES (Fig. 4) by ten linear hyperplanes in two convex regions.

PBTES SOC after the final time step is constrained to $s_{t_{n+1}}^{\text{TES}} = 0.5 \cdot S_{\max}^{\text{TES}}$. Furthermore, s_t^{TES} is soft-constrained to a critical value $S_{\text{crit}}^{\text{TES}} = 0.3 \cdot S_{\max}^{\text{TES}}$ via Eq. (22). This is a typical safety requirement for the operating plan.

Each UC run requires the current states of both the VES and the physical entity as initial values. To obtain the initial values, the service can query the data dimension of the DT platform via OBDA (see Section 2.2) and receive either the values themselves or the address to obtain them.

The UC problem of this service amounts 9693 continuous and 3982 binary variables with a constraint matrix of 36530 rows and 13675 columns, of which 140115 are non-zero. Every optimization service run reached the predefined MILP gap of 1% to the upper bound of the optimal solution before the maximum time of 5 h was reached.

3.1.7. MPC service

As outlined above, the MPC service is configured to operate at a higher frequency than the operation planning service to provide optimal control of the VES. In our implementation, the MPC service is triggered every 5 minutes and optimizes the operational schedule for the next 12 h. The PBTES SOC after the final time step $s_{t_{n+1}}^{\text{TES}}$ is constrained to the corresponding SOC from the operation planning service schedule at the time of t_{n+1}. This assures compliance with the long-term plan of the operation planning service. No other final constraints are set for the other components of the VES since their dynamic is considered to be relatively fast. The SOC of the steam storage s_t^{RSS} is soft-constrained to a critical value $S_{\text{crit}}^{\text{RSS}} = 0.2 \cdot S_{\max}^{\text{RSS}}$, i.e. to a slightly lower value than the operation planning service since the MPC service has a shorter frequency of recurrence. Other than the here-stated constraints, the MILP UC problem is equal to that of the operation planning service. The initial values are fetched equivalently to the operation planning service, see Section 3.1.6.

The UC problem of this service amounts 2352 continuous and 960 binary variables with a constraint matrix of 8453 rows and 3312 columns, of which 32433 are non-zero. Every optimization service run reached the predefined MILP gap of 0.01% to the upper bound of the optimal solution before the maximum time of 4 min was reached.

3.1.8. Day-ahead service

The implemented service follows a very simple procedure. It is called every day at 12:00 local time by a corresponding workflow. When called, the service fetches the last known VES schedule predicted by the operation planning service and fixes the electric turbine power, resulting from this schedule, for the 24 h of the next day. The fixed electric power in the database $P_j^{\text{el, fixed}}$ is then treated via Eq. (17) in the UC problem. This simulates the typical procedure of electricity procurement and marketing of industrial companies, i.e. sending the forecast to the energy supplier and thus committing the plant to this
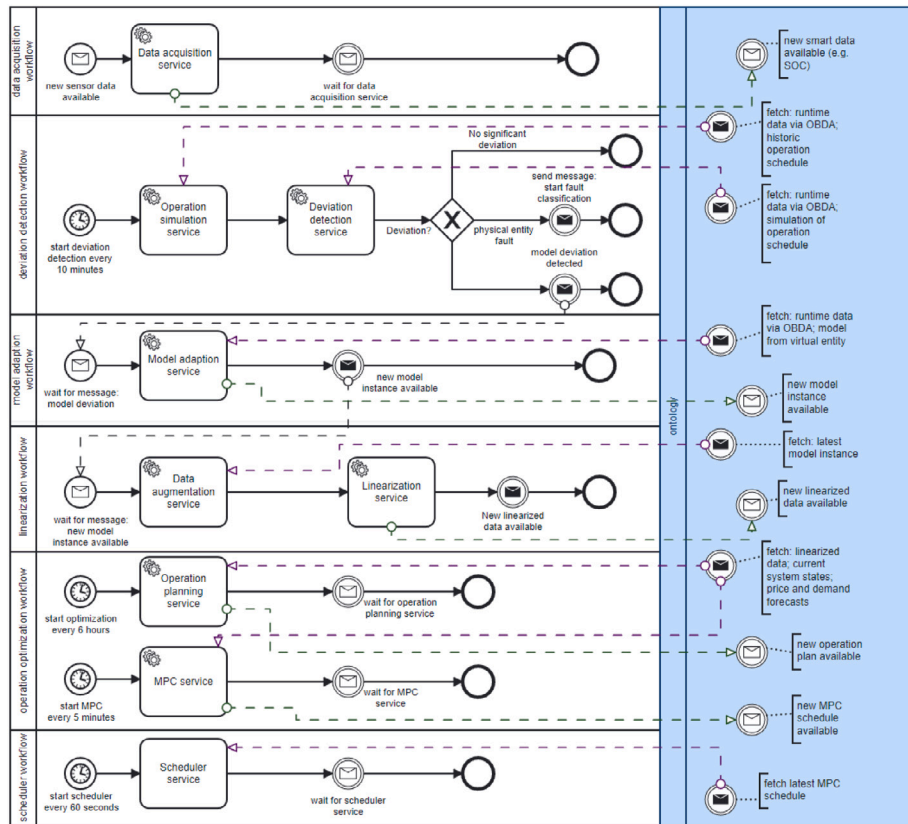
Fig. 6. BPMN diagram of the workflows orchestrated in the DT. The accentuated right-hand box visualizes the communication of individual services with the ontology of the DT platform.

load profile [88]. This DT service could be extended to also fulfill the automated load profile transmission to the energy supplier when applied in industrial applications.

3.1.9. Scheduler service

The scheduler service is responsible for sending the current set points of the optimized operation schedule to the SCADA system. It is called every 60 s and fetches the latest result schedule of the MPC service and searches for the values at the last time step before the current time. Power values are converted to an enthalpy difference based on the HTF mass flow and the temperature between the PBTES outlet and a fixed charging temperature. The corresponding values are then written to the OPC UA server of the SCADA system which directly controls the physical entity. This was implemented via Python OPC UA in this service. The OPC UA information model can be mapped once to an ontology in the DT platform's data dimension. After this, the node IDs of the respective control variables can be retrieved from the data dimension with a simple SPARQL query. This was demonstrated by Steindl et al. [89] and allows for a very flexible and scalable software implementation.

3.2. Digital twin workflows

As explained in Section 2.2, the runtime management of the DT services and the interaction between them is orchestrated by a workflow engine. Fig. 6 shows the implemented workflows and their communication with the ontology as a BPMN representation.

The right box in Fig. 6 represents the ontology, which is not part of BPMN but is included to highlight critical interaction between the individual services and the ontology. The solid arrows define the workflows, and the dashed arrows are visualizing the information flow between services and the ontology.

4. Results

4.1. Experimental procedure

The use case presented in Section 2.1 provided the means for experimental testing of the developed DT services and workflows for adaptive operation optimization. One week of typical operation of the industrial energy system, illustrated in Fig. 1, was assumed. The evaluation data is given in Appendix B. As explained in Section 2.5, the power and SOC values of the PBTES test rig are scaled by a constant factor to the MILP UC problem, and vice versa. We considered the fixed temperatures of 200 °C and 50 °C for charging and discharging, respectively. The scheduler service (see Section 3.1.9) calculates the mass flow necessary for a requested power value based on the temperature difference. These values are then controlled in the SCADA system via PID controllers. To simulate the continuous degradation of the PBTES in our lab, we introduced an artificial error. This error reduces the requested power value, hence the mass flow, by an increasing factor. The factor increases linearly from 0 at the start of the experiment to 0.6 after 7 days of operation. The artificial error was added to the scheduler service but not specified anywhere else within the DT platform.

4.2. Model adaption results

As discussed in Section 3.1.3, the model adaption service reacts to deviations between the physical entity's behavior and the virtual entity's behavior by adjusting a set of parameters θ. Based on the artificial error that reduced the mass flow provided by the ASU, we expect the two parameters η^+ and η^-, which are part of θ, to gradually decrease over time. We only considered these two parameters of θ to be variable during the evaluation and fixed the others to pre-identified
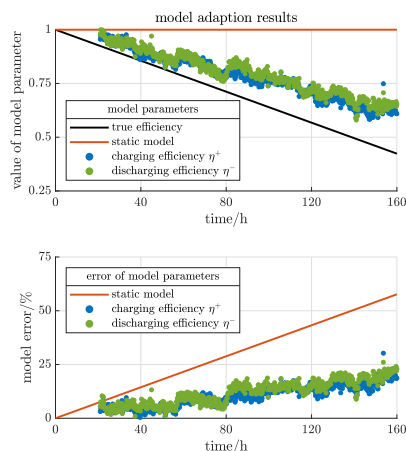
Fig. 7. Evaluation results of the model adaption service. Upper figure: Value of model parameters during the evaluation period. Lower figure: Error of model parameters of the adaptive model compared to a static model.

values. In Fig. 7, this expected behavior of a perfectly working model adaption service is plotted as a black solid line. At this point, it should be mentioned that in reality, the model adaption service will always lag behind this black line because the adaption procedure can only be done with historical data. This behavior can be observed in Fig. 7 in the blue and orange dots. These dots represent the values of η^+ and η^- that were fitted by the model adaption service on each execution. Although the model adaption is slightly lagging behind, it still detects the degradation of the thermal performance of the TES with acceptable accuracy. While the model error of a static model would increase to 60% over 7 days of operation, the model error remains well below 25% as a result of the model adaption. This information can be used by the other micro-services of the DT to improve the quality and accuracy of their output.

4.3. Virtual energy system operation

Here, an exemplary period of the VES operation during experimental operation is given. Fig. 8 illustrates 12 h of operation, $2\frac{1}{2}$ days into the experiment. The Figure depicts the heat flows and energy balances at the main conversion points specified in Fig. 1 in individual subplots (in the following numbered from top to bottom). The top-most subplot 1 shows the hot off-gas energy balance (Eq. (13)). Subplot 2 illustrates the PBTES operation. The energy balance within the saturated steam system (Eq. (18)), holds over subplots 3,4, and 6. Subplot 3 visualizes the total output power of the SG and the ratio of this power that is fed to the saturated steam system and to the superheater for subsequent turbine expansion. Subplot 4 illustrates the fulfillment of the process steam demand with direct saturated steam production and the RSS. The operation of the RSS is given in subplot 5. The decoupled heat from the turbine and steam system (Eq. (19)) is illustrated in subplot 6. The electric power output of the steam turbine, as well as the current electricity price, are illustrated in subplot 7.

4.4. Virtual energy system results

The successful model adaption during our experimental operation provides the basis for the efficient operation of the VES over long periods. Fig. 9 illustrates the predicted and achieved revenue during one week of VES operation. Here, the predicted revenue at a specific time corresponds to the mean revenue prediction by the MPC service that was made 12 h before for its prediction horizon. The given achieved revenue is the moving average over the same 12 h window resulting

from the actual VES simulation according to the PBTES test rig operation, as explained in Section 2.5. The VES operation is visualized in detail for an exemplary time period in Fig. 8 in Section 4.3.

It is visible that the prediction error remains in a typical magnitude of 10 to 20% during the operation period, despite the degradation of the PBTES power. The decreasing absolute value of the VES revenue toward the end of the week cannot be directly ascribed to the reduced PBTES capabilities but is mainly influenced by varying electricity prices and heat demands.

Further reduction of the prediction error of the MPC service is possible by the improvement of the experimental control. For example, we observed some delays in controlling the ASU of the test rig. A refined interval of the scheduler service (which was set to 60 s) could guarantee exact value setting according to the operation schedule. Furthermore, PID control of the HTF temperature entering the PBTES under varying mass flow is not trivial due to thermal inertia and leads to further fluctuations between the set power values and achieved values. These effects are amplified by the necessary downtime of our PBTES test rig, described in Section 2.4.4. Subplot 1 in Fig. 8 shows that we measured some PBTES discharging overshoots that were caused by the described delays. Similarly, the auxiliary gas burner was activated in the VES simulation when a certain charging power could not be achieved.

4.5. Digital twin approach

Despite the described options for further improvement, our experimental tests provided a successful proof of concept for the DT-based MILP model adaption. The automated adaption of the PBTES MILP model in the MPC and operation planning service ensured that efficient operational planning was not impaired. Even if further improvement of detailed methodical aspects of the DT services is required for a transfer from the laboratory environment to industrial application, the advantages of the DT approach are clear. As highlighted in our previous work on the DT platform [68] applied here, a message broker as the central communication hub and a microservice framework for managing inter-service workflows facilitate interoperability between different applications and the access and maintenance of distributed data sources. Adaptive operation optimization frameworks are complex, which is where the encapsulation into micro-services surpasses monolithic software implementations. Maintenance is facilitated when capitalizing on state-of-the-art software development frameworks such as Docker. This encapsulation in combination with overarching workflow management further fosters scalability such as the integration of new services.

Thus, we argue that the developed DT service structure in this work could provide an implementation template for at least basic economic energy management applications.

5. Conclusion and outlook

In this paper, an approach for automated adaptive modeling and operation optimization for industrial energy systems is presented. System components in the energy-intensive industry, such as the iron and steel sector, are exposed to harsh conditions, hence their performance tends to deteriorate. For effective operation planning, adaptive modeling could provide additional efficiency improvements. To address this challenge, we established a transferable and scalable methodology for this aim, based on innovative and promising digital twin (DT) technology. The foundation of this approach builds upon our previously developed five-dimensional DT platform. Several new DT micro-services, which encapsulate distinct functionality were established. This includes automated simulation model adaption, data augmentation, piecewise linearization of non-linear behavior, mixed integer linear programming (MILP) based operational optimization, and, live scheduling.
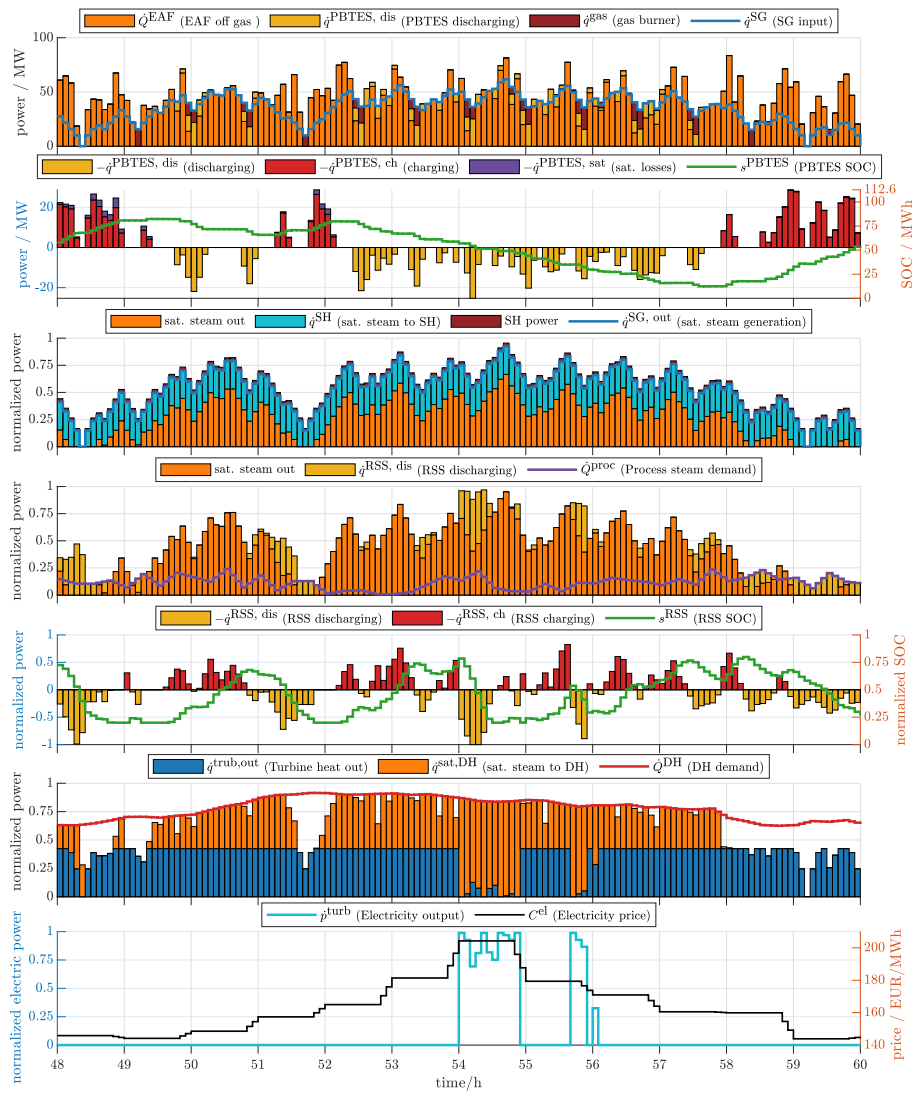
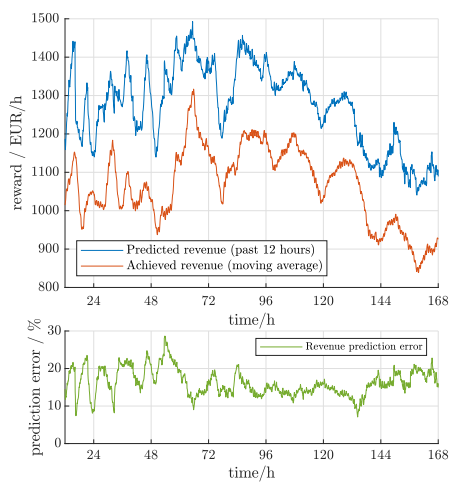**Fig. 8.** Exemplary 12 h of VES operation during the experimental evaluation.

Fig. 9. Results of one week VES operation. Upper figure: Predicted average revenue of the MPC service for the past 12 h prediction horizon (blue) and 12 h-moving average of the achieved revenue after PBTES operation and VES simulation (red). Lower figure: Deviation between predicted and achieved revenue.

We instantiated the developed services for a packed bed thermal energy storage (PBTES) test rig, acting as the physical entity of the DT, and validated them under consideration of a use case of waste heat recovery in steel production. Under the first experimental operation, we accomplished satisfactory results. The model adaption service proved adequate to keep the high-fidelity simulation model up to date for accurate and timely replication of the PBTES behavior. The data augmentation service and subsequent linearization service provide robust piecewise linear MILP models of the nonlinear PBTES behavior to be used for operational optimization and control. Thus, the prediction error of the MILP-based optimization compared to the actual operation did not increase, despite a continuously induced degradation of PBTES power. This approach facilitates efficient TES operation and thus contributes to flexible, low-emission industrial operation.

Additionally, we emphasize the advantage of the DT approach during engineering, system observation, and software maintenance. The DT platform facilitates scaling applications and implementing new services. The observation and administration of micro-services during operation proved very simple due to the use of software containers and workflow orchestration.

5.1. Outlook

Regarding the scope of this paper, two main overarching future research directions can be deduced: Further sophistication of DT technology, and, detailed investigations of PBTES integration for waste heat recovery in steel production under harsh operation.

Transferable methods for reliable deviation detection and fault classification will be highly relevant in the future. For example, Sleiti et al. [42] pointed out that data-driven approaches alone are not sufficient for a robust DT that detects deviations and triggers corresponding corrective actions. Rather, a multi-faceted approach is needed, e.g., by operating a physics-based model in parallel for verification purposes. Additionally, increased automation in initial MILP model creation based on system topology and properties could be futile, parallel to the work on automated control model identification [29,31,90]. For this, generic MILP frameworks are already available (see, e.g., [9, 76,91]) and the automated simulation model creation based on pipe and instrumentation diagrams has been demonstrated [92,93]. Fusing these approaches on a DT platform and using the methodology documented in the present paper could further contribute to widespread efficiency improvements.

CRediT authorship contribution statement

Lukas Kasper: Writing – review & editing, Writing – original draft, Visualization, Software, Methodology, Investigation, Formal analysis, Data curation, Conceptualization. **Paul Schwarzmayr:** Writing – review & editing, Writing – original draft, Visualization, Software, Methodology. **Felix Birkelbach:** Writing – review & editing, Formal analysis. **Florian Javernik:** Writing – review & editing, Resources, Conceptualization. **Michael Schwaiger:** Writing – review & editing, Resources, Conceptualization. **René Hofmann:** Writing – review & editing, Supervision, Project administration, Funding acquisition, Conceptualization.

Declaration of competing interest

The authors declare that they have no known competing financial interests or personal relationships that could have appeared to influence the work reported in this paper.

Data availability

The data that has been used is confidential.

Acknowledgments

Appendix A. Use case data

A.1. Evaluation data

Here, the representative input data, used for the use case evaluation, is presented.
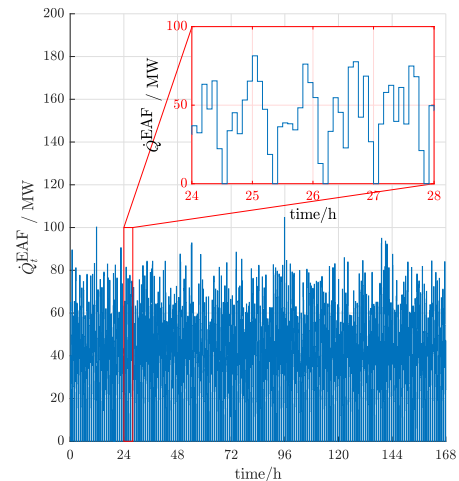

Fig. A.1. Assumed EAF waste heat data.

A.1.1. Electronic arc furnace waste heat

For the EAF waste heat, only limited literature data is available. We based our evaluation data on an EAF off-gas profile published by Steinparzer et al. [94], who provided off-gas flow and temperature measurements of one tap-to-tap (TTT) cycle of a $120\,t$ EAF. The profile shows temperature peaks of roughly $1200\,°C$ at typical volume flows of up to $200\,000\,Nm^3/h$, but also a sharp drop to $200\,°C$ during the EAF tapping. The authors stated in a later publication that the measurement data of this $120\,t$ EAF could be scaled up to a $150\,t$ EAF, resulting in $244\,kWh$ of waste heat per ton of steel produced [48].

We based our EAF use case data on these measurements and assumptions. Since we only considered absolute power values and no temperature levels in the VES model, we calculated the power profile from temperature and volume flow measurements from Steinparzer et al. [94]. However, we only considered off-gas temperatures above $400\,°C$ as usable, corresponding to a share of 0.944% of its total sensible thermal energy. This resulted in an average usable EAF excess heat of $41,47\,MW$ that was used to scale the given profile. The data was reproduced and modified by a slight statistical fluctuation and then downsampled to 5 minute intervals for the final use case profile. Fig. A.1 illustrates the EAF trajectory assumed for the use case evaluation.

A.1.2. Electricity and gas price

Of course, in day-ahead spot market participation, the quarter-hourly electricity prices are not only known until the price settlement, typically one day ahead. However, based on historical data and the weather forecast, it can be appropriately predicted via forecasting tools [88]. Thus, we assume known prices for a horizon of 48 hours. Weighted average Intra-day spot market prices in 15 min resolution from February 2023 were considered, retrieved from the European Power Exchange EPEX.[2] In the chosen time period, starting from Feb. 13, 2023, the electricity price ranged from 92 to $246\,€/MWh$, while daily spreads of typically more than $80\,€/MWh$ occurred, see Fig. A.2. Furthermore, we chose the Austrian wholesale natural gas import price from February 2023 as the representative gas price. It is available at E-Control[3] and was valued at $60\,€/MWh$.
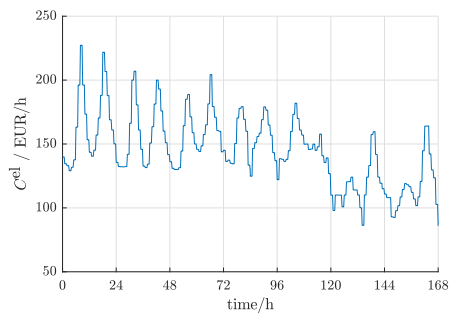

Fig. A.2. Electricity price during the use case evaluation period, retrieved from EPEX.[2]
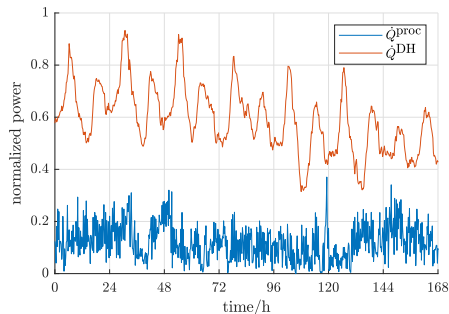

Fig. A.3. Process steam demand and heat demand during the use case evaluation period.

A.1.3. Steam and heat demand

The saturated steam demand as well as the internal and external heat demand chosen for the use case evaluation are based on measurements from the steel production plant Donawitz (Austria), from a typical winter period. Both steam and heat demand are visualized in Fig. A.3. Out of confidentiality, only normalized data can be provided here. The heat demand features a very stable base load but also typical twice-daily spikes. The steam demand features stronger volatility but can be roughly estimated based on the production schedule. The heat demand is about 4 to 5 times larger than the process steam demand.

A typical price for district heating reimbursement was assumed.

Appendix B. Virtual energy system parameters

Table B.1 lists the assumed unit parameters of the UC problem given in Section 2.4. In general, a slightly modified version of the MILP UC formulation presented in that section with additional design variables could be used for the design optimization of the energy system. However, this was not within the scope of this paper.

The system design and parameters were determined in coordination with our project partner and steel production plant operator voestalpine Stahl Donawitz GmbH. The use case, presented in detail in Section 2.1, corresponds to the current medium-term energy system adaption plans. The RSS system and the steam turbine already exist. We only consider feed-in to the low-pressure part of the turbine, which is mainly fed by the existing steam cycle. This steam cycle is fueled by post-combustion of the carbon monoxide-rich Linz-Donawitz (LD) converter gas from the existing blast furnace and LD converter routes. The auxiliary gas burner (considered to provide backup flexibility) and the SG were designed by empirical knowledge. Typical SG systems are restricted to maximum power ramping of 1-2 %/min of the maximum power [95]. A slight iteration of the presented use case could see a second or multiple PBTES installed in parallel. Without the downtime constraints that our PBTES test-rig exhibits, the auxiliary natural gas burner could potentially be spared or used only during start-up and emergency cases.

Table B.1
Assumed optimization problem parameters.

Parameter	Value
Auxiliary gas burner	
$\dot{Q}_{min}$	0 MW
$\dot{Q}_{max}$	50 MW
η_{gas}	0.99
Steam generator (SG)	
$\dot{Q}_{min}$	10 MW
$\dot{Q}_{max}$	70 MW
$\Delta\dot{Q}_{ramp}$	70 MW/h
η_{SG}	0.9
Steam turbine	
$\Delta\dot{Q}_{ramp}$	208 MW/h
$\eta_{turb, el}$	0.18
$\eta_{turb, out}$	0.98
Steam storage (RSS)	
$\dot{Q}_{max}$	20 MW
γ^{TES}	0.002 %/h
Packed bed thermal energy storage (PBTES)	
S^{TES}_{max}	112.6 MWh[a]
$\dot{Q}^{PBTES}_{max}$	39.0 MW[a]
$\dot{Q}^{PBTES}_{min}$	$^{100}/_{250}\,\dot{Q}^{PBTES}_{max}$
γ^{TES}	0.005 %/h

[a] These values correspond to the upscaled default values of the PBTES test rig. The default values are defined for the initial condition of the test rig. The actual values within the UC problem are retrieved from the virtual entity model.

The slack parameter value used in Eq. (22) was chosen as $A^{slack} = 10^6$. For details on appropriate slack parameter choice in energy system UC problems, see, e.g., [96].

References

[1] Global Carbon Project. Supplemental data of global carbon budget 2019 (version 1.0) [data set]. Global carbon project. Tech. rep., 2019, http://dx.doi.org/10.18160/gcp-2019.

[2] International Energy Agency (IEA). Greenhouse Gas Emissions from Energy Highlights. IEA; 2022, Available at: https://www.iea.org/data-and-statistics/data-product/greenhouse-gas-emissions-from-energy-highlights. Licence: Creative Commons Attribution CC BY-NC-SA 4.0.

[3] Miró L, Gasia J, Cabeza LF. Thermal energy storage (TES) for industrial waste heat (IWH) recovery: A review. Appl Energy 2016;179:284–301. http://dx.doi.org/10.1016/j.apenergy.2016.06.147.

[4] Martin V, Chiu NJ. Industrial applications of thermal energy storage systems. In: Advances in energy storage. John Wiley & Sons, Ltd; 2022, p. 729–47. http://dx.doi.org/10.1002/9781119239390.ch32.

[5] Pernsteiner D, Halmschlager V, Schirrer A, Hofmann R, Jakubek S. Efficient Sensitivity-Based Cooperation Concept for Hierarchical Multilayer Process Automation of Steam-Powered Plants. IEEE Access 2022;10:66844–61. http://dx.doi.org/10.1109/ACCESS.2022.3178436.

[6] Tatjewski P. Advanced control and on-line process optimization in multilayer structures. Annu Rev Control 2008;32(1):71–85. http://dx.doi.org/10.1016/j.arcontrol.2008.03.003.

[7] Abdou I, Tkiouat M. Unit Commitment Problem in Electrical Power System: A Literature Review. Int J Electr Comput Eng 2018;8(3):1357–72. http://dx.doi.org/10.11591/ijece.v8i3.pp1357-1372.

[8] Abdi H. Profit-based unit commitment problem: A review of models, methods, challenges, and future directions. Renew Sustain Energy Rev 2021;138:110504. http://dx.doi.org/10.1016/j.rser.2020.110504.

[9] Moser A, Muschick D, Gölles M, Nageler P, Schranzhofer H, Mach T, et al. A MILP-based modular energy management system for urban multi-energy systems: Performance and sensitivity analysis. Appl Energy 2020;261:114342. http://dx.doi.org/10.1016/j.apenergy.2019.114342.

[10] Moretti L, Martelli E, Manzolini G. An efficient robust optimization model for the unit commitment and dispatch of multi-energy systems and microgrids. Appl Energy 2020;261:113859. http://dx.doi.org/10.1016/j.apenergy.2019.113859.

[11] Gan L, Yang T, Wang B, Chen X, Hua H, Dong ZY. Three-stage coordinated operation of steel plant-based multi-energy microgrids considering carbon reduction. Energy 2023;278:127639. http://dx.doi.org/10.1016/j.energy.2023.127639.

[12] Zhang Q, Grossmann IE. Enterprise-wide optimization for industrial demand side management: Fundamentals, advances, and perspectives. Chem Eng Res Des 2016;116:114–31. http://dx.doi.org/10.1016/j.cherd.2016.10.006, Process Systems Engineering - A Celebration in Professor Roger Sargent's 90th Year.

[13] Dowling AW, Kumar R, Zavala VM. A multi-scale optimization framework for electricity market participation. Appl Energy 2017;190:147–64. http://dx.doi.org/10.1016/j.apenergy.2016.12.081.

[14] Muschick D, Zlabinger S, Moser A, Lichtenegger K, Gölles M. A multi-layer model of stratified thermal storage for MILP-based energy management systems. Appl Energy 2022;314:118890. http://dx.doi.org/10.1016/j.apenergy.2022.118890.

[15] Kotzur L, Nolting L, Hoffmann M, Groß T, Smolenko A, Priesmann J, et al. A modeler's guide to handle complexity in energy systems optimization. Adv Appl Energy 2021;4:100063. http://dx.doi.org/10.1016/j.adapen.2021.100063.

[16] Milan C, Stadler M, Cardoso G, Mashayekh S. Modeling of non-linear CHP efficiency curves in distributed energy systems. Appl Energy 2015;148:334–47. http://dx.doi.org/10.1016/j.apenergy.2015.03.053.

[17] Koller M, Hofmann R, Walter H. MILP model for a packed bed sensible thermal energy storage. Comput Chem Eng 2019;125:40–53. http://dx.doi.org/10.1016/j.compchemeng.2019.03.007.

[18] Yu J, Petersen N, Liu P, Li Z, Wirsum M. Hybrid modelling and simulation of thermal systems of in-service power plants for digital twin development. Energy 2022;260:125088. http://dx.doi.org/10.1016/j.energy.2022.125088.

[19] Soualhi M, El Koujok M, Nguyen KT, Medjaher K, Ragab A, Ghezzaz H, et al. Adaptive prognostics in a controlled energy conversion process based on long- and short-term predictors. Appl Energy 2021;283:116049. http://dx.doi.org/10.1016/j.apenergy.2020.116049.

[20] Zhang H, Li G, An X, Ye X, Wei G, Yu A. Numerical study on the erosion process of the low temperature economizer using computational fluid dynamics-discrete particle method. Wear 2020;450–451:203269. http://dx.doi.org/10.1016/j.wear.2020.203269.

[21] Castro PM, Dalle Ave G, Engell S, Grossmann IE, Harjunkoski I. Industrial demand side management of a steel plant considering alternative power modes and electrode replacement. Ind Eng Chem Res 2020;59(30):13642–56. http://dx.doi.org/10.1021/acs.iecr.0c01714.

[22] He B, Liu L, Zhang D. Digital Twin-Driven Remaining Useful Life Prediction for Gear Performance Degradation: A Review. J Comput Inf Sci Eng 2021;21(3):030801. http://dx.doi.org/10.1115/1.4049537.

[23] Chaichan MT, Kazem HA, Ibrahim SI, Radhi AA, Mahmoud BK, Ali AJ. Photovoltaic panel type influence on the performance degradation due dust accumulation. IOP Conf Ser Mater Sci Eng 2020;928(2):022092. http://dx.doi.org/10.1088/1757-899X/928/2/022092.

[24] Subotić V, Menzler NH, Lawlor V, Fang Q, Pofahl S, Harter P, et al. On the origin of degradation in fuel cells and its fast identification by applying unconventional online-monitoring tools. Appl Energy 2020;277:115603. http://dx.doi.org/10.1016/j.apenergy.2020.115603.

[25] Liu Z, Chen H, Zhang T. Review on system mitigation strategies for start-stop degradation of automotive proton exchange membrane fuel cell. Appl Energy 2022;327:120058. http://dx.doi.org/10.1016/j.apenergy.2022.120058.

[26] Lyu C, Song Y, Zheng J, Luo W, Hinds G, Li J, et al. In situ monitoring of lithium-ion battery degradation using an electrochemical model. Appl Energy 2019;250:685–96. http://dx.doi.org/10.1016/j.apenergy.2019.05.038.

[27] Adesusi OM, Adetunji OR, Kuye SI, Musa AI, Erinle TJ, Gbadamosi-Olatunde OB, et al. A comprehensive review of the materials degradation phenomena in solid-liquid phase change materials for thermal energy storage. Int J Thermofluids 2023;18:100360. http://dx.doi.org/10.1016/j.ijft.2023.100360.

[28] Knobloch K, Ulrich T, Bahl C, Engelbrecht K. Degradation of a rock bed thermal energy storage system. Appl Therm Eng 2022;214:118823. http://dx.doi.org/10.1016/j.applthermaleng.2022.118823.

[29] Pattison RC, Touretzky CR, Johansson T, Harjunkoski I, Baldea M. Optimal Process Operations in Fast-Changing Electricity Markets: Framework for Scheduling with Low-Order Dynamic Models and an Air Separation Application. Ind Eng Chem Res 2016;55(16):4562–84. http://dx.doi.org/10.1021/acs.iecr.5b03499.

[30] Kelley MT, Baldick R, Baldea M. Demand response scheduling under uncertainty: Chance-constrained framework and application to an air separation unit. AIChE J 2020;66(9):e16273. http://dx.doi.org/10.1002/aic.16273.

[31] Kelley MT, Pattison RC, Baldick R, Baldea M. An MILP framework for optimizing demand response operation of air separation units. Appl Energy 2018;222:951–66. http://dx.doi.org/10.1016/j.apenergy.2017.12.127.

[32] Lu X, Cannon M, Koksal-Rivet D. Robust adaptive model predictive control: Performance and parameter estimation. Internat J Robust Nonlinear Control 2021;31(18):8703–24. http://dx.doi.org/10.1002/rnc.5175.

[33] Adetola V, DeHaan D, Guay M. Adaptive model predictive control for constrained nonlinear systems. Systems Control Lett 2009;58(5):320–6. http://dx.doi.org/10.1016/j.sysconle.2008.12.002.

[34] Forbes MG, Patwardhan RS, Hamadah H, Gopaluni RB. Model Predictive Control in Industry: Challenges and Opportunities. IFAC-PapersOnLine 2015;48(8):531–8. http://dx.doi.org/10.1016/j.ifacol.2015.09.022, 9th IFAC Symposium on Advanced Control of Chemical Processes ADCHEM 2015.

[35] Lu Y, Liu C, Wang KI-K, Huang H, Xu X. Digital Twin-driven smart manufacturing: Connotation, reference model, applications and research issues. Robot Comput-Integr Manuf 2020;61:101837. http://dx.doi.org/10.1016/j.rcim.2019.101837.

[36] Yu W, Patros P, Young B, Klinac E, Walmsley TG. Energy digital twin technology for industrial energy management: Classification, challenges and future. Renew Sustain Energy Rev 2022;161:112407. http://dx.doi.org/10.1016/j.rser.2022.112407.

[37] Negri E, Fumagalli L, Macchi M. A Review of the Roles of Digital Twin in CPS-based Production Systems. Procedia Manuf 2017;11:939–48. http://dx.doi.org/10.1016/j.promfg.2017.07.198.

[38] Cimino C, Negri E, Fumagalli L. Review of digital twin applications in manufacturing. Comput Ind 2019;113:103130. http://dx.doi.org/10.1016/j.compind.2019.103130.

[39] Liu M, Fang S, Dong H, Xu C. Review of digital twin about concepts, technologies, and industrial applications. J Manuf Syst 2021;58:346–61. http://dx.doi.org/10.1016/j.jmsy.2020.06.017.

[40] Kritzinger W, Karner M, Traar G, Henjes J, Sihn W. Digital Twin in manufacturing: A categorical literature review and classification. IFAC-PapersOnLine 2018;51(11):1016–22. http://dx.doi.org/10.1016/j.ifacol.2018.08.474.

[41] Josifovska K, Yigitbas E, Engels G. Reference Framework for Digital Twins within Cyber-Physical Systems. In: 2019 IEEE/ACM 5th international workshop on software engineering for smart cyber-physical systems. Institute of Electrical and Electronics Engineers Inc; 2019, p. 25–31. http://dx.doi.org/10.1109/SEsCPS.2019.00012.

[42] Sleiti AK, Kapat JS, Vesely L. Digital twin in energy industry: Proposed robust digital twin for power plant and other complex capital-intensive large engineering systems. Energy Rep 2022;8:3704–26. http://dx.doi.org/10.1016/j.egyr.2022.02.305.

[43] Bagherian MA, Mehranzamir K, Pour AB, Rezania S, Taghavi E, Nabipour-Afrouzi H, et al. Classification and Analysis of Optimization Techniques for Integrated Energy Systems Utilizing Renewable Energy Sources: A Review for CHP and CCHP Systems. Processes 2021;9(2). http://dx.doi.org/10.3390/pr9020339.

[44] Sun Y, Tian S, Ciais P, Zeng Z, Meng J, Zhang Z. Decarbonising the iron and steel sector for a 2° C target using inherent waste streams. Nature Commun 2022;13(1):297. http://dx.doi.org/10.1038/s41467-021-27770-y.

[45] International Energy Agency. Iron and Steel Technology Roadmap. Tech. rep., Paris: International Energy Agency; 2020, URL https://www.iea.org/reports/iron-and-steel-technology-roadmap. [Accessed 12 June 2023].

[46] Wang P, Ryberg M, Yang Y, et al. Efficiency stagnation in global steel production urges joint supply- and demand-side mitigation efforts. Nature Commun 2021;12:2066. http://dx.doi.org/10.1038/s41467-021-22245-6.

[47] Kirschen M, Risonarta V, Pfeifer H. Energy efficiency and the influence of gas burners to the energy related carbon dioxide emissions of electric arc furnaces in steel industry. Energy 2009;34(9):1065–72. http://dx.doi.org/10.1016/j.energy.2009.04.015.

[48] Keplinger T, Haider M, Steinparzer T, Patrejko A, Trunner P, Haselgrübler M. Dynamic simulation of an electric arc furnace waste heat recovery system for steam production. Appl Therm Eng 2018;135:188–96. http://dx.doi.org/10.1016/j.applthermaleng.2018.02.060.

[49] Nardin G, Meneghetti A, Dal Magro F, Benedetti N. PCM-based energy recovery from electric arc furnaces. Appl Energy 2014;136:947–55. http://dx.doi.org/10.1016/j.apenergy.2014.07.052.

[50] Inayat A. Current progress of process integration for waste heat recovery in steel and iron industries. Fuel 2023;338:127237. http://dx.doi.org/10.1016/j.fuel.2022.127237.

[51] voestalpine Stahl Donawitz GmbH. greentec steel. 2023, URL https://www.voestalpine.com/stahldonawitz/en/quality-and-environment/greentec-steel/. [Accessed 12 June 2023].

[52] Steinparzer T, Haider M, Fleischanderl A, Hampel A, Enickl G, Zauner F. Heat exchangers and thermal energy storage concepts for the off-gas heat of steelmaking devices. J Phys Conf Ser 2012;395(1):012158. http://dx.doi.org/10.1088/1742-6596/395/1/012158.

[53] Dal Magro F, Savino S, Meneghetti A, Nardin G. Coupling waste heat extraction by phase change materials with superheated steam generation in the steel industry. Energy 2017;137:1107–18. http://dx.doi.org/10.1016/j.energy.2017.04.051.

[54] Bostick GL. 14 - Operation and controls. In: Eriksen VL, editor. Heat Recovery Steam Generator Technology. Woodhead Publishing; 2017, p. 287–319. http://dx.doi.org/10.1016/B978-0-08-101940-5.00014-2.

[55] Manente G, Ding Y, Sciacovelli A. A structured procedure for the selection of thermal energy storage options for utilization and conversion of industrial waste heat. J Energy Storage 2022;51:104411. http://dx.doi.org/10.1016/j.est.2022.104411.

[56] Gautam A, Saini R. A review on sensible heat based packed bed solar thermal energy storage system for low temperature applications. Sol Energy 2020;207:937–56. http://dx.doi.org/10.1016/j.solener.2020.07.027.

[57] Gautam A, Saini R. A review on technical, applications and economic aspect of packed bed solar thermal energy storage system. J Energy Storage 2020;27:101046. http://dx.doi.org/10.1016/j.est.2019.101046.

[58] Xie B, Baudin N, Soto J, Fan Y, Luo L. Chapter 10 - Thermocline packed bed thermal energy storage system: a review. In: Jeguirim M, editor. Renewable energy production and distribution. Advances in renewable energy technologies, vol. 1, Academic Press; 2022, p. 325–85. http://dx.doi.org/10.1016/B978-0-323-91892-3.24001-6.

[59] Marti J, Geissbühler L, Becattini V, Haselbacher A, Steinfeld A. Constrained multi-objective optimization of thermocline packed-bed thermal-energy storage. Appl Energy 2018;216:694–708. http://dx.doi.org/10.1016/j.apenergy.2017.12.072.

[60] Bause T, Campana F, Filippini L, Foresti A, Monti N, Pelz T. Cogeneration with ORC at elbe-stahlwerke feralpi EAF shop. In: Proceedings of the iron & steel technology conference and exposition, Indianapolis, in, USA. 2014, p. 5–8, URL http://www.hreii.eu/demo/public/AISTech%202014_Paper_Bause_Cogeneration%20with%20ORC%20at%20Elbe_Stahlwerke%20Feralpi%20EAF%20Shop.pdf. [Accessed 12 June 2023].

[61] Guézennec A-G, Huber J-C, Patisson F, Sessiecq P, Birat J-P, Ablitzer D. Dust formation in Electric Arc Furnace: Birth of the particles. Powder Technol 2005;157(1):2–11. http://dx.doi.org/10.1016/j.powtec.2005.05.006, 4th French Meeting on Powder Science and Technology.

[62] Keplinger T, Haider M, Steinparzer T, Trunner P, Patrejko A, Haselgrübler M. Modeling, Simulation, and Validation with Measurements of a Heat Recovery Hot Gas Cooling Line for Electric Arc Furnaces. Steel Res Int 2018;89(6):1800009. http://dx.doi.org/10.1002/srin.201800009.

[63] Schwarzmayr P, Birkelbach F, Walter H, Javernik F, Schwaiger M, Hofmann R. Packed bed thermal energy storage for waste heat recovery in the iron and steel industry: An experimental study on powder hold-up and pressure drop. 2023, http://dx.doi.org/10.48550/arXiv.2307.01585.

[64] Dong X, Pinson D, Zhang S, Yu A, Zulli P. Gas–powder flow and powder accumulation in a packed bed: I. Experimental study. Powder Technol 2004;149(1):1–9. http://dx.doi.org/10.1016/j.powtec.2004.09.040.

[65] Hollands K, Sullivan H. Pressure drops across rock bed thermal storage systems. Sol Energy 1984;33(2):221–5. http://dx.doi.org/10.1016/0038-092X(84)90241-X.

[66] Singh H, Saini R, Saini J. A review on packed bed solar energy storage systems. Renew Sustain Energy Rev 2010;14(3):1059–69. http://dx.doi.org/10.1016/j.rser.2009.10.022.

[67] Steindl G, Stagl M, Kasper L, Kastner W, Hofmann R. Generic Digital Twin Architecture for Industrial Energy Systems. Appl Sci 2020;10(24). http://dx.doi.org/10.3390/app10248903.

[68] Kasper L, Birkelbach F, Schwarzmayr P, Steindl G, Ramsauer D, Hofmann R. Toward a Practical Digital Twin Platform Tailored to the Requirements of Industrial Energy Systems. Appl Sci 2022;12(14). http://dx.doi.org/10.3390/app12146981, Section "Energy Science and Technology". Special Issue "Industry 4.0 Technologies Supporting the Energy Transition".

[69] Schwarzmayr P, Birkelbach F, Kasper L, Hofmann R. Development of a Digital Twin Platform for Industrial Energy Systems. In: Applied energy symposium: MIT A+B. Cambridge, USA; 2022, p. 1–6. http://dx.doi.org/10.46855/energy-proceedings-9974.

[70] Tao F, Zhang M, Nee AYC. Chapter 3 - Five-Dimension Digital Twin Modeling and Its Key Technologies. In: Tao F, Zhang M, Nee AYC, editors. Digital Twin Driven Smart Manufacturing. Academic Press; 2019, p. 63–81. http://dx.doi.org/10.1016/B978-0-12-817630-6.00003-5.

[71] Hogan A, Blomqvist E, Cochez M, D'amato C, Melo GD, Gutierrez C, et al. Knowledge Graphs. ACM Comput Surv 2021;54(4). http://dx.doi.org/10.1145/3447772.

[72] Bagosi T, Calvanese D, Hardi J, Komla-Ebri S, Lanti D, Rezk M, et al. The Ontop Framework for Ontology Based Data Access. In: Zhao D, Du J, Wang H, Wang P, Ji D, Pan JZ, editors. The Semantic Web and Web Science. Berlin, Heidelberg: Springer; 2014, p. 67–77. http://dx.doi.org/10.1007/978-3-662-45495-4_6.

[73] Schwarzmayr P, Birkelbach F, Walter H, Hofmann R. Standby efficiency and thermocline degradation of a packed bed thermal energy storage: An experimental study. Appl Energy 2023;337:120917. http://dx.doi.org/10.1016/j.apenergy.2023.120917.

[74] Majidi M, Mohammadi-Ivatloo B, Anvari-Moghaddam A. Optimal robust operation of combined heat and power systems with demand response programs. Appl Therm Eng 2019;149:1359–69. http://dx.doi.org/10.1016/j.applthermaleng.2018.12.088.

[75] Fuhrmann F, Schirrer A, Kozek M. Model-predictive energy management system for thermal batch production processes using online load prediction. Comput Chem Eng 2022;163:107830. http://dx.doi.org/10.1016/j.compchemeng.2022.107830.

[76] Halmschlager V, Hofmann R. Assessing the potential of combined production and energy management in Industrial Energy Hubs – Analysis of a chipboard production plant. Energy 2021;226:120415. http://dx.doi.org/10.1016/j.energy.2021.120415.

[77] Koller M, Hofmann R. Mixed-Integer Linear Programming Formulation of Combined Heat and Power Units for the Unit Commitment Problem. J Sustain Dev Energy Water Environ Syst 2018;6(4):755–69. http://dx.doi.org/10.13044/j.sdewes.d6.0207.

[78] Weber T, Strobel N, Kohne T, et al. Realistic modeling of a combined heat and power plant in the context of mixed integer linear programming. Energy Inf 2018;1:27. http://dx.doi.org/10.1186/s42162-018-0037-z.

[79] Merkel D. Docker: Lightweight linux containers for consistent development and deployment. Linux J 2014;2014(239):2.

[80] Lofberg J. YALMIP: A toolbox for modeling and optimization in MATLAB. In: 2004 IEEE international conference on robotics and automation. 2004, p. 284–9. http://dx.doi.org/10.1109/CACSD.2004.1393890.

[81] Schwarzmayr P, Birkelbach F, Walter H, Hofmann R. Study on the Standby Characteristics of a Packed Bed Thermal Energy Storage: Experimental Results and Model Based Parameter Optimization. In: Proceedings of the ASME 2023 power conference. Long Beach, CA; 2023, http://dx.doi.org/10.1115/POWER2023-108578.

[82] Birkelbach F, Huber D, Hofmann R. Piecewise linear approximation for MILP leveraging piecewise convexity to improve performance. 2023, http://dx.doi.org/10.48550/arXiv.2309.10372.

[83] Birkelbach F. MILPtools. 2022, [Gitlab repository]. Available at: https://gitlab.tuwien.ac.at/iet/public/milptools.

[84] Dias LS, Pattison RC, Tsay C, Baldea M, Ierapetritou MG. A simulation-based optimization framework for integrating scheduling and model predictive control, and its application to air separation units. Comput Chem Eng 2018;113:139–51. http://dx.doi.org/10.1016/j.compchemeng.2018.03.009.

[85] Fuhrmann F, Windholz B, Schirrer A, Knöttner S, Schenzel K, Kozek M. Energy management for thermal batch processes with temporarily available energy sources– Laboratory experiments. Case Stud Therm Eng 2022;39:102473. http://dx.doi.org/10.1016/j.csite.2022.102473.

[86] Valibeygi A, Konakalla SAR, Callafon Rd. Predictive Hierarchical Control of Power Flow in Large-Scale PV Microgrids With Energy Storage. IEEE Trans Sustain Energy 2021;12(1):412–9. http://dx.doi.org/10.1109/TSTE.2020.3001260.

[87] Polimeni S, Meraldi L, Moretti L, Leva S, Manzolini G. Development and experimental validation of hierarchical energy management system based on stochastic model predictive control for Off-grid Microgrids. Adv Appl Energy 2021;2:100028. http://dx.doi.org/10.1016/j.adapen.2021.100028.

[88] Hadera H, Harjunkoski I, Sand G, Grossmann IE, Engell S. Optimization of steel production scheduling with complex time-sensitive electricity cost. Comput Chem Eng 2015;76:117–36. http://dx.doi.org/10.1016/j.compchemeng.2015.02.004.

[89] Steindl G, Frühwirth T, Kastner W. Ontology-based OPC UA data access via custom property functions. In: 2019 24th IEEE International Conference on Emerging Technologies and Factory Automation (ETFA). 2019, p. 95–101. http://dx.doi.org/10.1109/ETFA.2019.8869436.

[90] Tsay C, Kumar A, Flores-Cerrillo J, Baldea M. Optimal demand response scheduling of an industrial air separation unit using data-driven dynamic models. Comput Chem Eng 2019;126:22–34. http://dx.doi.org/10.1016/j.compchemeng.2019.03.022.

[91] Krien U, Schönfeldt P, Launer J, Hilpert S, Kaldemeyer C, Pleßmann G. oemof.solph—A model generator for linear and mixed-integer linear optimisation of energy systems. Softw Impacts 2020;6:100028. http://dx.doi.org/10.1016/j.simpa.2020.100028.

[92] Steindl G, Kastner W. Ontology-Based Model Identification of Industrial Energy Systems. In: 2020 IEEE 29th International Symposium on Industrial Electronics . 2020, p. 1217–23. http://dx.doi.org/10.1109/ISIE45063.2020.9152386.

[93] Sierla S, Azangoo M, Fay A, Vyatkin V, Papakonstantinou N. Integrating 2D and 3D Digital Plant Information Towards Automatic Generation of Digital Twins. In: 2020 IEEE 29th International Symposium on Industrial Electronics. 2020, p. 460–7. http://dx.doi.org/10.1109/ISIE45063.2020.9152371.

[94] Steinparzer T, Haider M, Zauner F, Enickl G, Michele-Naussed M, Horn AC. Electric Arc Furnace Off-Gas Heat Recovery and Experience with a Testing Plant. Steel Res Int 2014;85(4):519–26. http://dx.doi.org/10.1002/srin.201300228.

[95] Hofmann R, Panuschka S, Beck A. A simultaneous optimization approach for efficiency measures regarding design and operation of industrial energy systems. Comput Chem Eng 2019;128:246–60. http://dx.doi.org/10.1016/j.compchemeng.2019.06.007.

[96] Fuhrmann F, Schirrer A, Kozek M. MPC for Process Heat Supply Systems: Considering Load Prediction Uncertainty Caused by Human Operators. In: Pierucci S, Manenti F, Bozzano GL, Manca D, editors. 30th European Symposium on Computer Aided Process Engineering. Computer Aided Chemical Engineering, vol. 48, Elsevier; 2020, p. 1219–24. http://dx.doi.org/10.1016/B978-0-12-823377-1.50204-4.